# HYDRAULIC RAM SHOCK WAVE AND CAVITATION EFFECTS ON AIRCRAFT FUEL CELL SURVIVABILITY

Dwight Patrick Holm

# THESIS

HYDRAULIC RAM SHOCK WAVE
AND CAVITATION EFFECTS ON AIRCRAFT
FUEL CELL SURVIVABILITY

by

Dwight Patrick Holm

Thesis Advisor: Allen E. Fuhs

September 1973

Hydraulic Ram Shock Wave and Cavitation Effects

on Aircraft Fuel Cell Survivability

by

Dwight Patrick Holm
Lieutenant (junior grade), United States Navy
B.S., University of Kansas, 1970

Submitted in partial fulfillment of the
requirements for the degree of

MASTER OF SCIENCE IN AERONAUTICAL ENGINEERING

from the

NAVAL POSTGRADUATE SCHOOL
September 1973

ABSTRACT

Hydraulic ram is the dynamic loading of fuel tanks when impacted by bullets or other projectiles. During impact and penetration of the fuel cell, intense pressure waves are generated by the projectile.

A ballistic range was built and experimental testing was conducted to study hydraulic ram phenomena. A 0.22 caliber rifle was used to accelerate projectiles at velocities in the range of 0.38 km/sec into a transparent, water filled tank. Shape and intensity of the shock wave pressure pulse induced as a result of projectile impact were determined using a dual shadowgraph system. Peak pressures were found to be as high as $4.50 \times 10^3$ kg/cm$^2$. The rate of energy transfer to the fluid by the projectile was determined experimentally and compared with analytical predictions. A characteristic time was defined establishing the separation point between the shock and cavity phases of hydraulic ram.

TABLE OF CONTENTS

LIST OF FIGURES

## LIST OF SYMBOLS

| | |
|---|---|
| $a$ | Sound speed in gas |
| $A$ | Projectile frontal area |
| $c_o$ | Sound speed in water |
| $C_D$ | Drag coefficient |
| c.g. | Center of gravity |
| c.p. | Center of pressure |
| $D$ | Drag force on the projectile |
| $E$ | Kinetic energy of the projectile |
| $E_o$ | Impact kinetic energy of the projectile |
| $m$ | Projectile mass |
| $P$ | Fluid pressure |
| $P_o$ | Initial pressure |
| $P_\infty$ | Ambient pressure |
| $r$ | Radial distance |
| $r_p$ | Piston radius |
| $R$ | Cavity radius |
| $R_o$ | Initial cavity radius |
| $t$ | Time |
| $t'$ | Dimensionless time |
| $u$ | Fluid velocity |
| $V$ | Projectile velocity |
| $V_o$ | Projectile impact velocity |

| | |
|---|---|
| $V_s$ | Shock wave velocity |
| $V$ | Volume |
| $x$ | Distance coordinate |
| $X$ | $R_o/R$ |
| $\alpha$ | $P_o/(\gamma - 1)\, P_\infty$ |
| $\gamma$ | Ratio of specific heats |
| $\rho$ | Density of gas |
| $\rho_o$ | Initial density of the gas |
| $\rho_f$ | Density of fluid |
| $\phi$ | Fluid potential function |

## ACKNOWLEDGEMENTS

The author is indebted to Laird Stanton and Bob Smith for their generous assistance in the design and construction of the delay circuitry. Appreciation is also extended to the Aeronautics Department Technician Staff for their help in the construction of the test apparatus. The author would also like to gratefully acknowledge the invaluable counseling of his thesis advisor, Professor Allen E. Fuhs, during the preparation of this report. This project was funded by Naval Weapons Center, China Lake; Dr. Eric Lundstrom is project monitor.

# I. INTRODUCTION

When enclosed fluid containers are impacted by high speed projectiles, severe damage can occur as a result of the phenomenon known as hydraulic ram. Numerous experimental investigations of the hydraulic ram effect have been conducted including research by Cole, Stepka, Lundstrom, and Yurkovich (Refs. 1-7). An investigation, presently being conducted at the Naval Postgraduate School, graphically demonstrates this effect. The damage shown in Figs. 1 and 2 occurred when a plexiglas test tank, simulating an aircraft fuel cell, was impacted by a 2.92 gram, 0.222 caliber projectile traveling at a velocity of 0.889 kilometers per second (2910 ft/sec).

In determining aircraft survivability the destruction due to hydraulic ram becomes of paramount importance and, in fact, is the major cause of damage when an aircraft is hit by small arms fire or warhead fragments (Ref. 6). This is further substantiated by the fact that fuel tank (or cell) components comprise the greatest portion of the target area in modern attack and fighter aircraft. There are numerous examples of catastrophic failure of fuel cells which were subjected to ballistic impact (Ref. 6). Other kill modes due to hydraulic ram include: fuel starvation, explosion and fire, and damage to aircraft components adjacent to the fuel cell. In space flight the hazard of meteoroid impact into liquid propellant tanks is another area of concern because an impact of sufficient energy could cause catastrophic bursting of the tank wall.

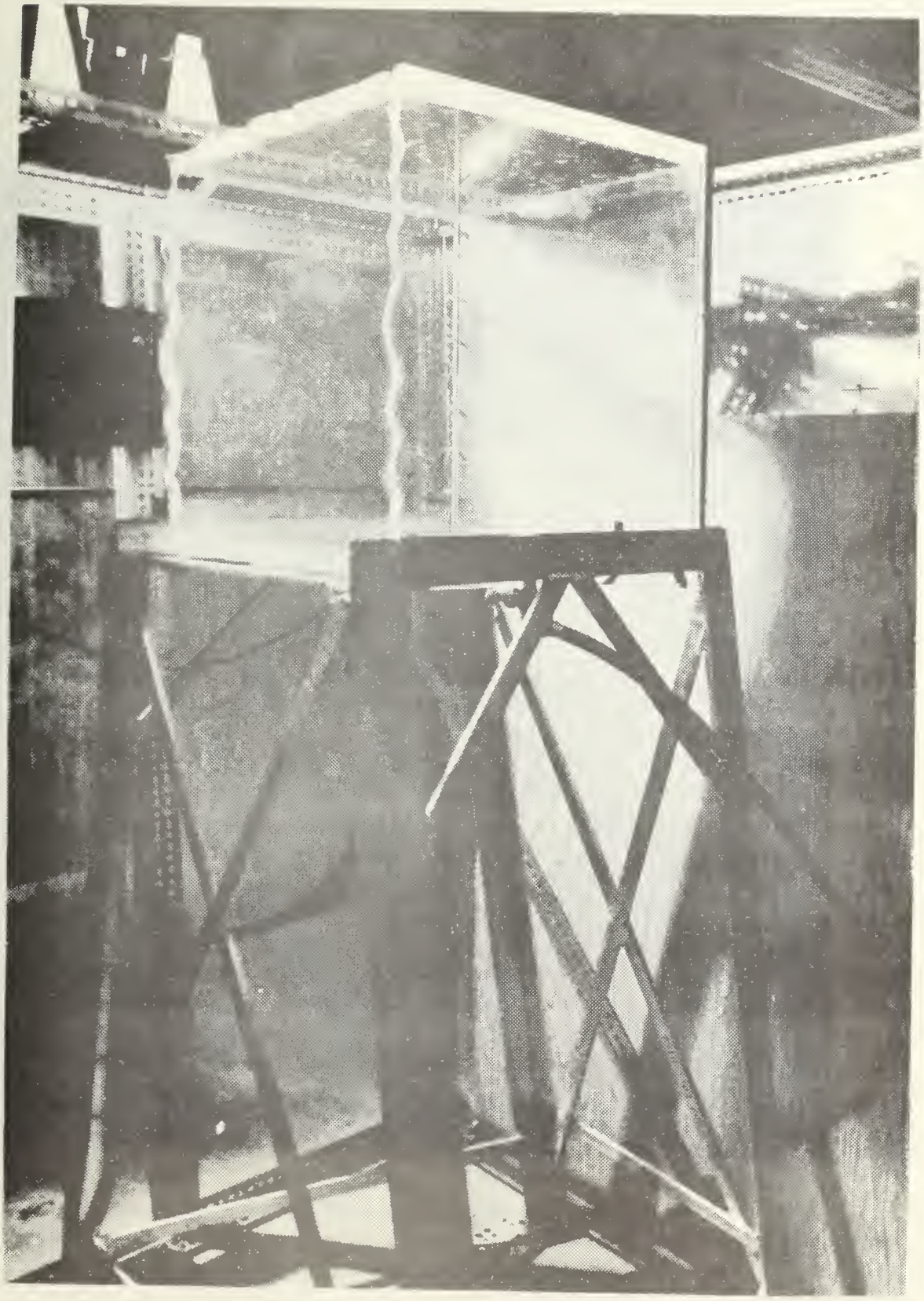

Fig. 1 Hydraulic Ram Damage to the Test Tank.

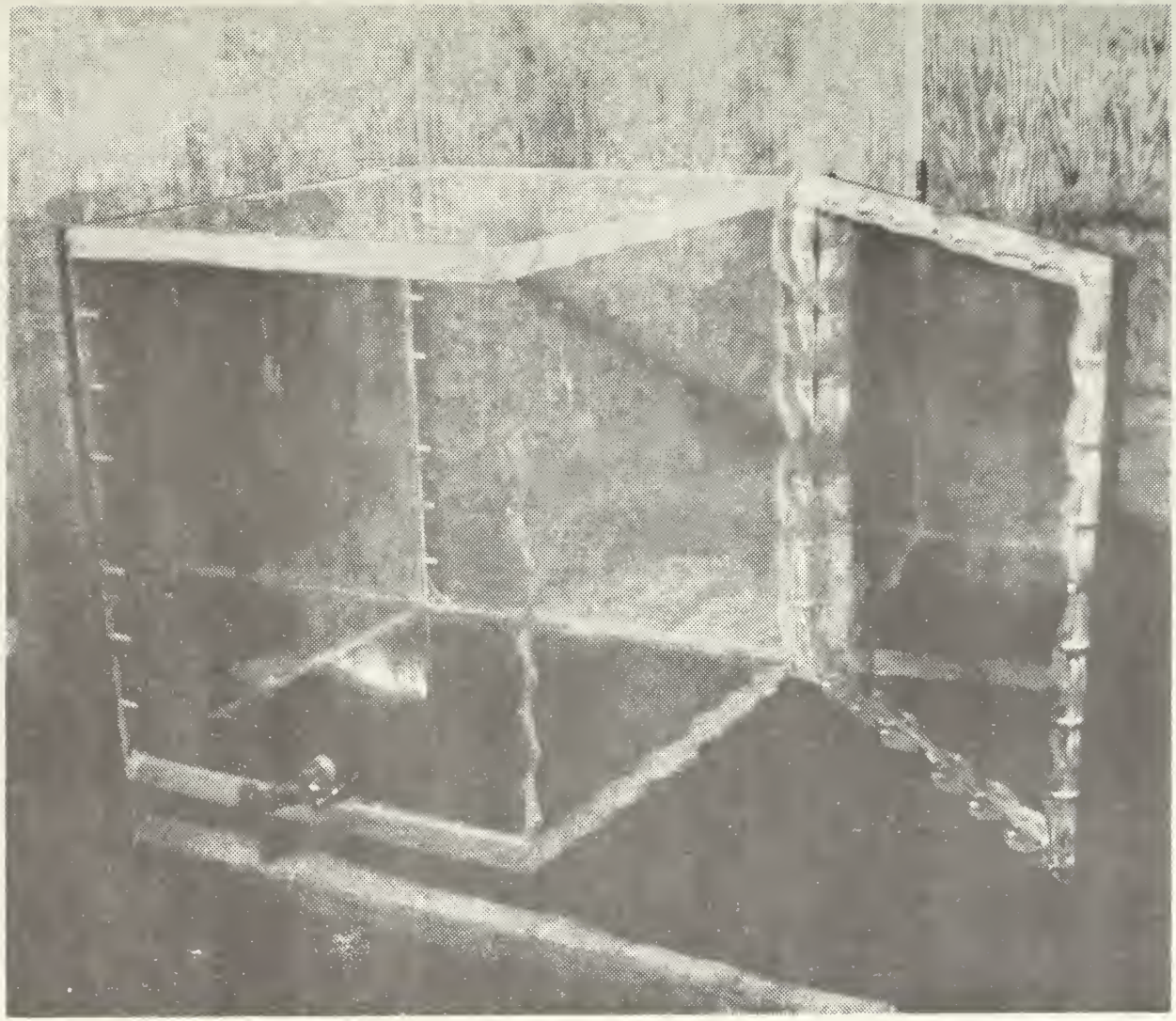

Fig. 2 Hydraulic Ram Damage.

Concern with the aircraft fuel tank vulnerability problem did not begin with the recent air conflict in Southeast Asia. Since World War II, there have been efforts to reduce hydraulic ram damage to an acceptable level; however, with few exceptions, the efforts have been "trial and error" procedures. The result has been that many schemes have been tried, but none has been found fully effective. While not being satisfactory, many of these ideas have shown promise in defeating at least some of the hydraulic ram components. Several important fuel tank defense schemes were developed and tested by North American Rockwell during the late 1960's. These concepts are published as a survivable fuel tank systems handbook (Ref. 8) in which the basic design features are divided into "intrinsic" and "parasitic" defense concepts. Intrinsic defense concepts utilize specific aircraft configuration considerations to reduce system vulnerability. Examples would be: tank shapes with smooth contours, low surface-to-volume ratios, few corners and fittings, and fuel system considerations to isolate the cell. This type of defense concept is thus "intrinsic" to the basic airframe design and can be effectively applied only when the aircraft is in preliminary design stages. Parasitic defense concepts include protective devices and systems added to the aircraft primarily to enhance fuel cell survivability; these concepts include elements not otherwise essential to normal aircraft function. Examples are: self-sealing tanks and the addition of reticulated foam inside fuel cells to reduce the hydraulic ram effect.

The purpose of this study is the investigation of the hydraulic ram phenomenon itself. Fuel tank response to projectile penetration cannot be fully understood without a prior comprehension of the individual hydraulic ram components. This understanding, plus a knowledge of events which occur during the damaging process, must be obtained in order to change the tank arrangement in such a way as to properly influence the damage. Once fuel cells are protected against this type of threat, overall aircraft vulnerability will be lessened.

## II. NATURE OF THE PROBLEM

It has been found (Refs. 6 and 7) that the loading and deformation of fuel tanks by hydraulic ram is a combination of a number of events. These events, known as the hydraulic ram components, are outlined in Figs. 3 and 4. The column on the left in Fig. 3 describes the motion of the projectile as it passes through the tank. When the projectile enters the tank, a shock wave is formed and cracks may develop due to the high pressure and stresses near the entry point. As the projectile traverses the fluid, high pressure is generated, and energy is imparted to the fluid through projectile drag. This increased energy sets the fluid in motion forming a cavity. Both the fluid motion and the subsequent cavity formation and collapse impose stresses on the tank walls. Finally, if the projectile has sufficient kinetic energy, it will exit the tank. As it exits from the tank, a local area of compressed fluid is formed, and cracks are produced around the exit hole. As shown in Fig. 4, the wall loadings plus the cracks at the entry and exit points can result in various types of damage.

Excluding crack formation due to the actual entry and exit of the projectile, hydraulic ram is composed of two main separable effects; a shock phase and a drag or cavity phase, both of which are important in causing damage. During the initial impact, the projectile impulsively accelerates the fluid, thus generating an intense pressure field of short

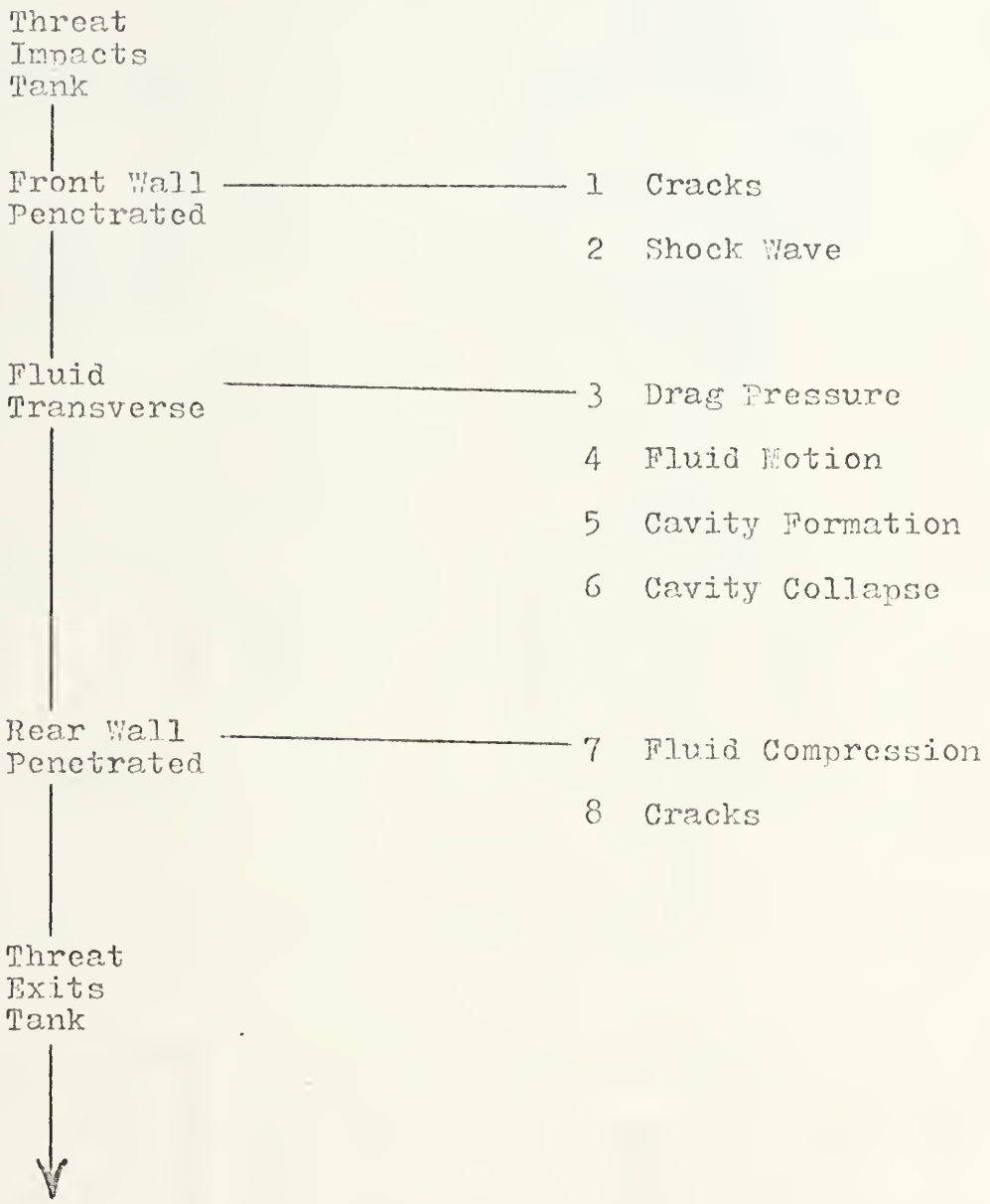


Fig. 3 Outline of Hydraulic Ram Phenomenon adapted from Reference 10.

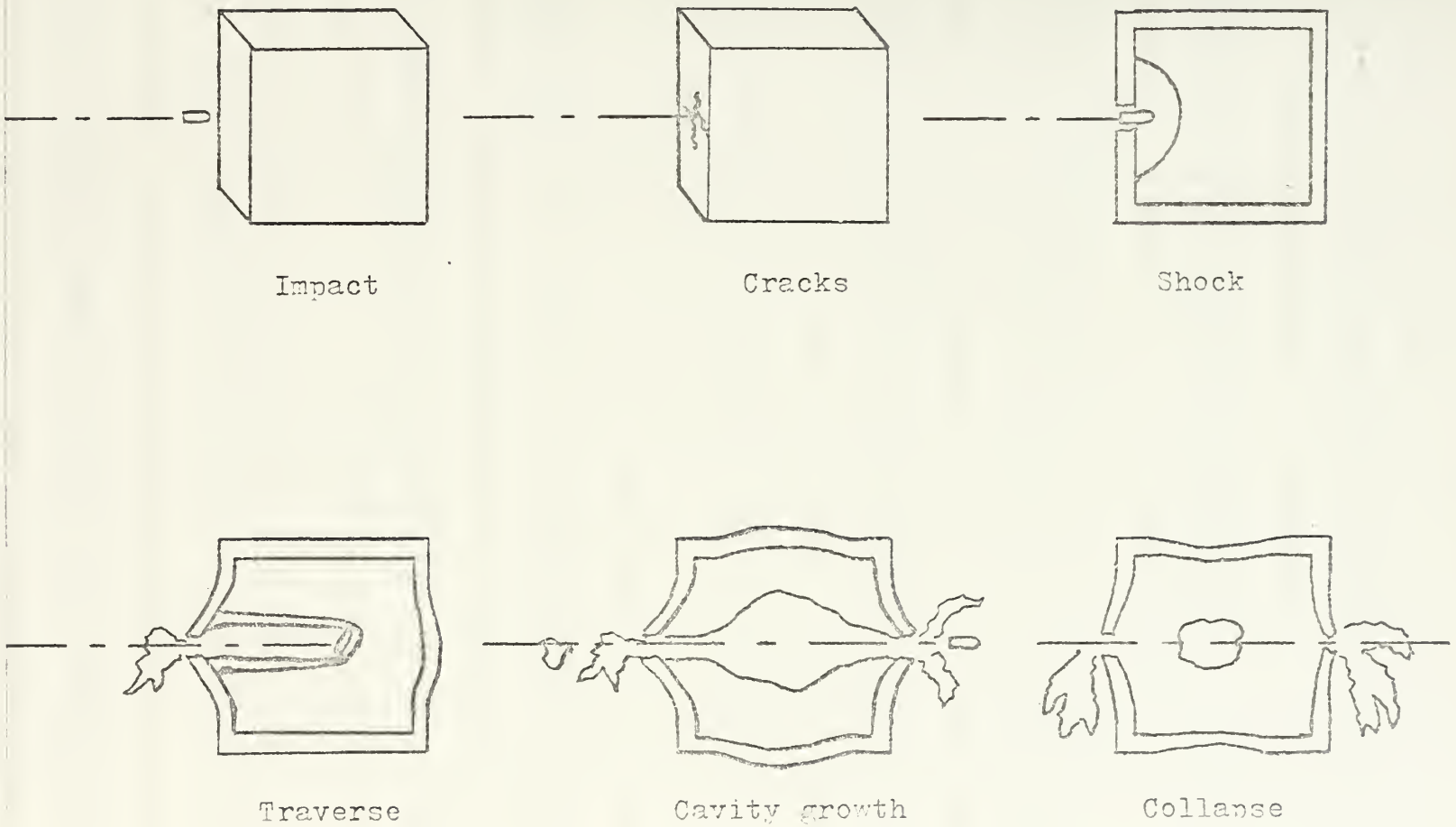


Fig. 4 Hydraulic Ram Damage Sequence
adapted from Reference 10.

duration. This phenomenon is characteristic of the shock phase of hydraulic ram. The contribution of the shock-phase pressure pulse toward fuel cell failure is particularly important in the case of small, high velocity projectile impact. After passage of the projectile, pressure phenomena become increasingly complex due to: 1) multiple sources of the pressure, 2) reflections of the pressure waves, 3) motion of the fluid, and 4) tank wall deflection. These events lead to the formation of a cavity and mark the beginning of the cavity phase. The formation of a large cavity behind the projectile is the most striking phenomenon associated with ballistic penetration of fluids. The pressure field produced by the cavity formation and collapse is of low amplitude but long duration and has a dynamic behavior loosely analogous to that of a cavity formed by an underwater explosion.

The shock and cavity phases that have just been described have been treated in this analysis as two separate effects. A clearer understanding of the relationship between the shock and cavity phenomena can be gained by considering the projectile energy transfer time-history as shown in Fig. 5 (Ref. 9). Two separate regions can be distinguished which correspond to the two main effects present in hydraulic ram. The first region is characterized by a high energy transfer from the projectile to the fluid. It is while the projectile is in this region that the shock wave is formed and begins to propagate. The second region is characterized by a lower and nearly constant rate of energy transfer to the fluid. This second region, which lasts for the remaining time that the

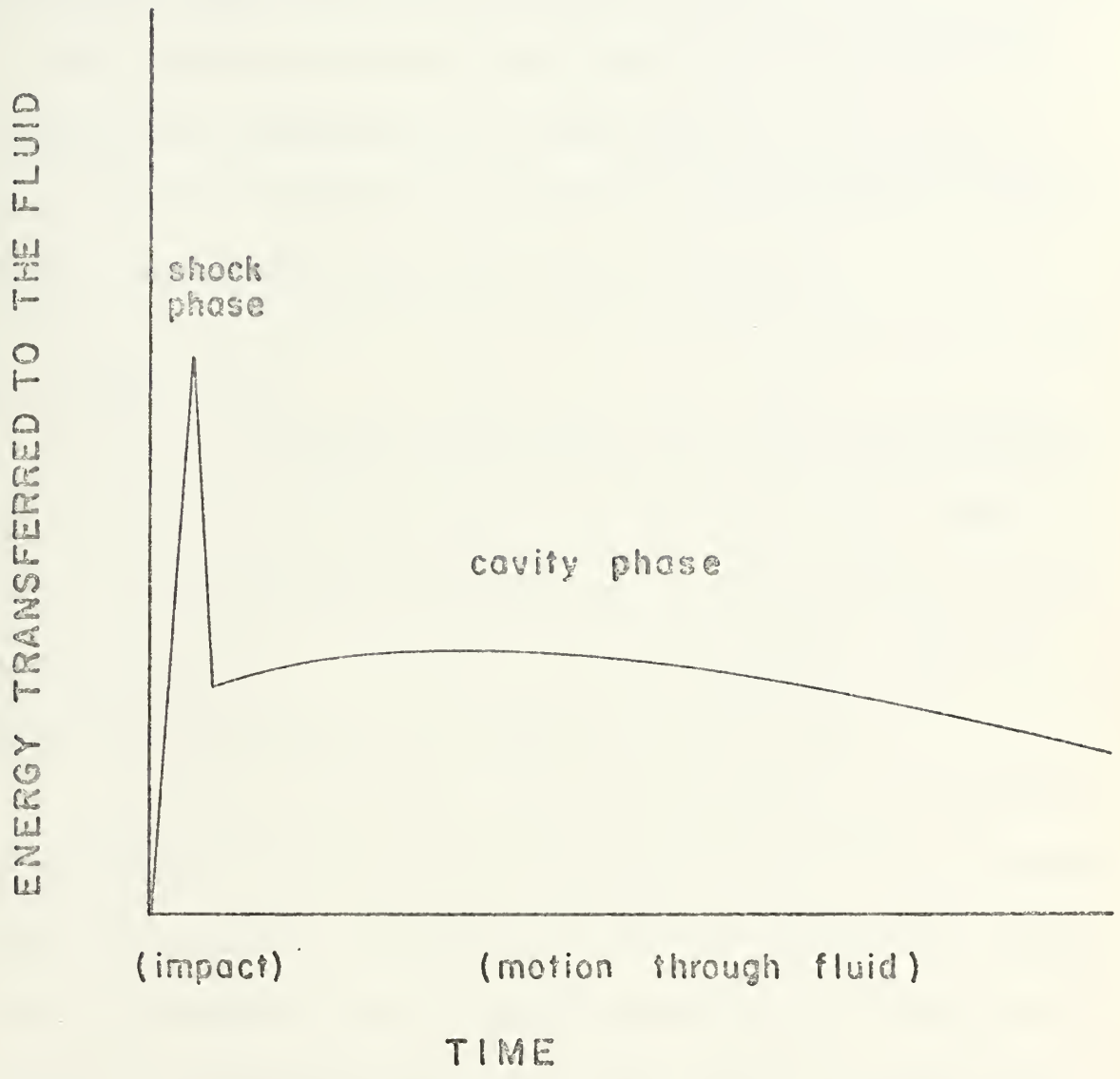


Fig. 5 Energy Transferred to the Fluid by a Projectile Versus Time.

projectile is traversing the tank, is known as the drag or cavity phase. In this phase, projectile energy is transformed into the kinetic energy of fluid motion which leads to the formation of a cavity.

The work here was done to further the development of analytical methods used in understanding the complex hydraulic ram phenomenon. Once an ability to predict the response of fuel cells to ballistic impact exists, overall aircraft survivability will be enhanced.

## A. SHOCK PHASE

Shock wave formation and propagation due to projectile penetration into a fluid-filled tank will result in very high local pressures which can cause catastrophic failure of the entry wall. This result has been shown experimentally (Refs. 2 - 5), and it provides the motivation behind the study of the shock phase of the hydraulic ram phenomenon.

The shock or impact phase can itself be regarded as a succession of interrelated events which will be discussed in their order of occurrence. When a fuel tank wall is impacted by a high velocity projectile, dynamic stresses are generated and transmitted through the wall. These stresses are due to the puncturing and cratering action from the projectile impact and take the form of compressive and circumferential bending stress in the wall (Ref. 3). As the projectile is penetrating the tank wall, it impulsively accelerates the fluid directly behind the impact point. An instant before impact the fluid is at rest, and in the next instant it is traveling at the velocity of the projectile. This sudden acceleration of the

fluid by the projectile during impact and penetration generates an intense pressure field bounded by a shock wave. Tank wall stresses are induced by this pressure field which, when added to the dynamic stresses due to cratering, can cause catastrophic failure of the entry wall. The shock wave pressure field expands in a hemispherical shape away from the impact point with a velocity greater than the acoustic speed of the fluid. Both the velocity of the shock front and the intensity of the related pressure field vary directly with the amount of energy transferred to the fluid by the projectile during the initial impact (Refs. 3 and 4). The amount of impact energy which is transferred to the fluid is dependent on a number of parameters including: projectile size, density, and geometric shape; tank wall material and construction; and the physical properties of the fluid (Ref. 5). In general, for any given time after impact, small high-velocity projectiles lose a larger part of their impacting kinetic energy than more massive, low velocity projectiles (Ref. 2). This observation indicates that for the same impact kinetic energies, a more damaging pressure pulse for wall fracture will result from impact by small high velocity projectiles than with more massive low velocity projectiles.

Although the peak pressure due to projectile impact is high, the pressure field is rapidly weakened because of the geometric expansion of the shock wave. An experimental example of this pressure attenuation is provided by Stepka (Ref. 2). Impact with a 0.9 gram steel cylinder at an impact velocity of 4.27 km/sec resulted in pressures of 4.63

giganewtons per square meter ($0.67 \times 10^6$ lb/in$^2$) at a distance of 1.9 centimeters (3/4 inch) from the impact point. However, the pressure at the shock front decayed to ambient values within 13 centimeters (5 inches) from the impact point. These results indicate that even for impacts with high velocity and high kinetic energy projectiles, the side or rear walls of any large tank would not be subjected to significant pressures due to the shock phase.

In summary, the shock phase of hydraulic ram is characterized by an intense pressure field of short duration. It is essentially a "point source" energy release and results in an expanding, hemispherically shaped, pressure wave front that emanates from the point of impact. The kinetic energy of the projectile is the most important parameter in determining the speed of propagation and strength of the shock front. The shock-phase pressure pulse contributes to fuel cell failure mainly in the case of small high velocity projectile impact.

B. CAVITY PHASE.

After the initial impact with the tank, which is responsible for the shock phase, the projectile continues to decelerate as it traverses through the fluid. It is during this time that the cavity phase of the hydraulic ram phenomenon is generated.

When an object moves through a fluid, it feels a resistance known as "drag." Drag forces are due to an uneven pressure distribution and viscous effects of the fluid. If the pressure distribution is integrated in

the direction of motion, the resulting force is known as "pressure drag." Compared with the drag due to viscous effects, pressure drag is the predominant drag force (90%) at projectile velocities (Ref. 10).

Drag is usually expressed in terms of a nondimensional "drag coefficient," which is dependent on the density of the fluid, as well as on the size, velocity, and geometric shape of the object. A typical drag coefficient for a high-velocity projectile is 0.15, but this value will increase by a factor of ten or more for a tumbled or flattened projectile (Ref. 10). In the analytical study of hydraulic ram, this coefficient can be used to account for the much greater pressure generating capability of deformed and tumbled projectiles.

Applied to the projectile surface, the drag forces generate a pressure gradient between the projectile and the fluid. This causes the surrounding fluid to move away from the surface of the projectile. In this manner, the projectile energy is gradually transformed into the kinetic energy of fluid motion. In contrast to the shock phase, the fluid is accelerated gradually rather than impulsively so the peak pressure is lower. However, the duration of the pressure pulse is much longer. Once a sufficient amount of energy is transferred to the fluid, it will form a void, known as a cavity, around and behind the projectile. The cavity which is formed would be a complete vacuum except for two phenomena. It is filled with fluid vapors from pressure vaporization effects and with entrained air from the projectile entry and exit points. After passage of the projectile, the hydraulic ram cavity continues to

expand until all fluid momentum has been dissipated. The momentum is lost to the surrounding fluid by fluid pressures which resist cavity growth. These same pressures including pressure due to the force of gravity cause the cavity to collapse. Collapse of the over-expanded cavity would be exactly opposite to cavity growth except for the presence of fluid vapors and trapped air. These vapors and air act as a spring to make complete collapse impossible. From this point on the cavity acts much like an explosion cavity; the cavity oscillations generate low amplitude but long duration pressure pulses. The cavity may oscillate through several cycles until the energy of the fluid is dissipated. The pulse width and peak pressure produced by the cavity oscillation depend on the total energy transferred to the fluid, the amount of gas trapped in the cavity, and the shape of the cavity itself (Ref. 6). Pressure pulses due to the cavity phase of hydraulic ram are generally more damaging than those of the shock phase due to their longer duration.

The rate of energy transfer to the fluid is the major factor that determines the severity of hydraulic ram. Projectile kinetic energy dissipation is proportional to the square of the velocity decay as the projectile traverses the fluid. This indicates that the projectile deceleration time-history as it passes through a fluid is of great importance in the study of hydraulic ram.

## III. ANALYTICAL APPROACH TO CAVITY OSCILLATION AND PRESSURE FIELD

Two analytical problems were investigated concerning the oscillatory cavity phase of hydraulic ram. The first problem involved the derivation of a method for predicting the collapse time for a cavity when the vapor pressure within was negligible. The assumption applied to this problem was that the cavity contained a vacuum. The second problem carried the same basic analysis even further by modeling the oscillation of a cavity with finite internal pressures. This cavity was found to behave much like a spring in its oscillatory pattern. Isentropic compression and expansion were the basic assumptions used in the second problem.

### A. COLLAPSE OF A CAVITY CONTAINING A VACUUM VERSUS TIME

Potential flow relationships for an incompressible fluid were used in the formulation of this problem. The cavity was assumed to be spherical in shape with an initial radius $R_o$. $R = R(t)$ describes the motion of the fluid - gas surface which travels at the velocity u. From continuity, the flow field is described by

$$\frac{\partial}{\partial r}\left(r^2 u\right) = 0 \qquad (1)$$

where r is the instantaneous cavity radius. Potential flow theory along with the momentum equation for an incompressible fluid was

used to obtain the equation of motion for a cavity. It was found (Appendix A) that:

$$R\ddot{R} + \frac{3}{2}\dot{R}^2 = \frac{P(R,t) - P_\infty}{\rho} \qquad (2)$$

where P (R, t) was the pressure in the fluid at the cavity wall. Assuming that P (R, t) was known, equation (2) was manipulated into the general form

$$\dot{R}^2 = \frac{2}{R^3}\int_{R_o}^{R}\left(\frac{P(R,0)}{\rho} - \frac{P_\infty}{\rho}\right)R^2\,dR \qquad (3)$$

For the first problem with $R = R_o$, $\dot{R}_o = 0$ and $P(R, 0) = 0$, the integral yields the time for the cavity to reach a fraction of its initial radius

$$t = \frac{-R_o}{\sqrt{\frac{2}{3}\frac{P_\infty}{\rho}}}\int_{X}^{1}\frac{X^{3/2}\,dX}{\sqrt{1-X^3}} \qquad (4)$$

where $X = R / R_o$. This equation was numerically integrated by computer. The result describes the motion of a spherical cavity with time when the cavity contains a vacuum and starts at some initial radius $R_o$. Solutions for two cavities with varying initial conditions are shown in the computer outputs of Figs. 6 and 7. These plots give valuable insight into the frequency response and an order of magnitude for the time to cavity collapse. Figure 6 gives a time to collapse of 0.011 seconds

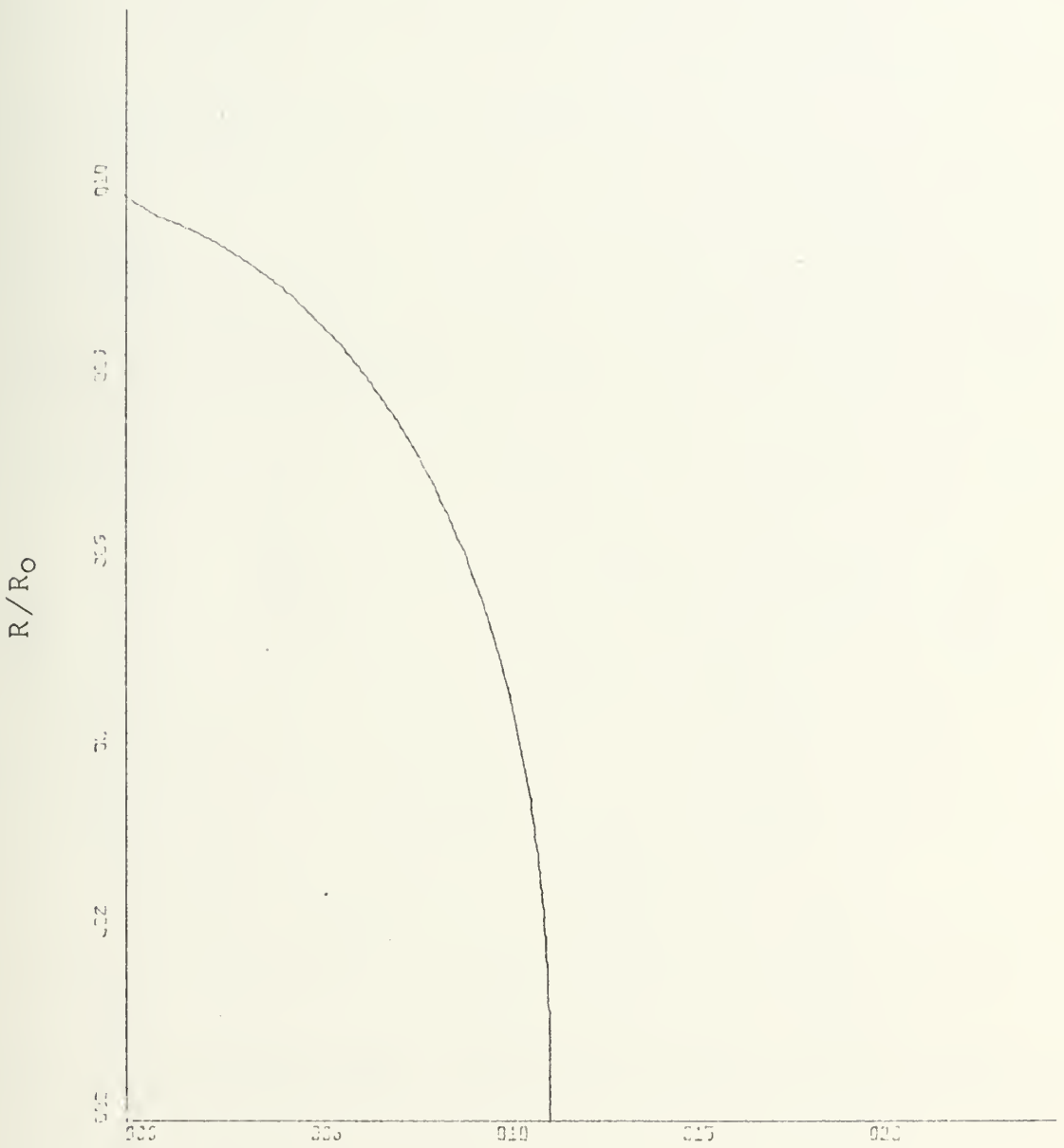


Fig. 6 Cavity Collapse Time from an Initial Radius of 0.5 Foot.

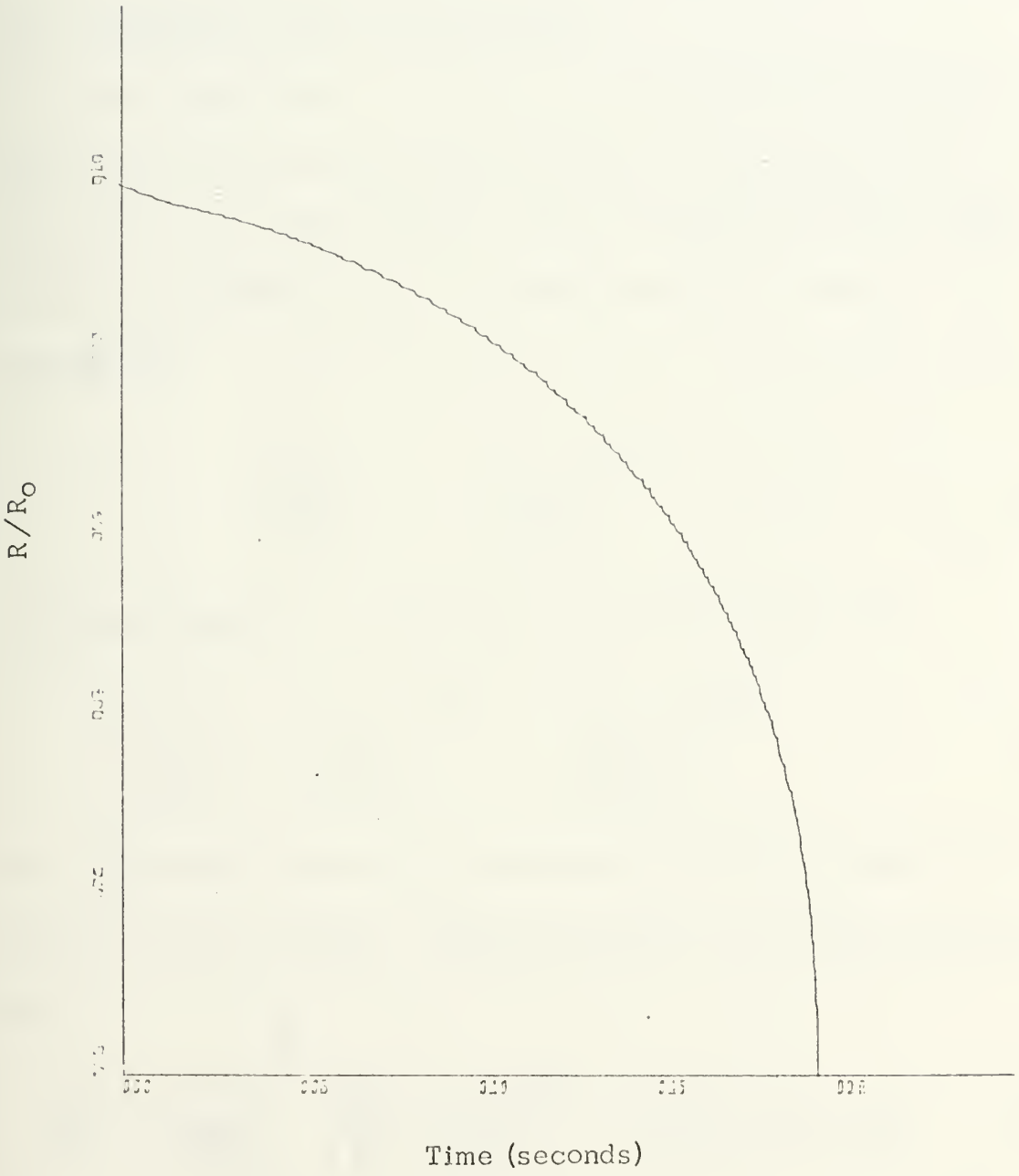


Fig. 7 Cavity Collapse Time from an Initial Radius of 1.0 Foot.

for a cavity with the parameters: $R_o = 0.5$ ft, $P_\infty = 2200$ lb/ft$^2$, and $\rho_f = 1.94$ slug/ft$^3$. Figure 7 is the solution to the problem with the following initial conditions: $R_o = 1.0$ ft, $P_\infty = 2500$ lb/ft$^2$, and $\rho_f = 1.60$ slug/ft$^3$.

## B. ISENTROPIC CAVITY OSCILLATIONS

The second problem, which assumed the cavity was filled with gas and followed a series of isentropic compressions and expansions, was approached in a manner similar to the first problem. Starting with $R(0) = R_o$ and $P(R, 0) = P_o$, it was known that for isentropic compression

$$\left(\frac{P}{P_o}\right) = \left(\frac{\rho}{\rho_o}\right)^{\gamma} \tag{5}$$

which when applied to a homogeneous gas-filled sphere yields

$$\left(\frac{P}{P_o}\right) = \left(\frac{\rho}{\rho_o}\right)^{\gamma} = \left(\frac{R_o}{R}\right)^{3\gamma} \tag{6}$$

This relationship was derived by assuming that $\dot{R} << a$, where a was the speed of sound in the gas. Combining equations (3) and (6) it was found that

$$\dot{R}^2 = \frac{2}{R^3}\int_{R_o}^{R}\left[\frac{P_o}{\rho}\left(\frac{R_o}{R}\right)^{3\gamma} - \frac{P_\infty}{\rho}\right]R^2\,dR \tag{7}$$

A dimensionless time was defined as

$$t' = \frac{t\sqrt{\frac{2}{3}\frac{P_\infty}{\rho}}}{R_o} \tag{8}$$

and combined with equation (7). The final expression for cavity motion is

$$t' = \int_X^1 \frac{\alpha X}{X^2\left[X^3(\alpha+1) - \alpha X^{3\gamma} - 1\right]^{1/2}} \tag{9}$$

where $\alpha = P_o/(\gamma - 1)P_{oo}$ and $X = R_o/R$. Equation (9) was solved through the use of a numerical integration computer program. The cavity radius, represented by $X = R_o/R$, was found to oscillate about the equilibrium position $X = 1$. This response was expected, since the cavity started at an initial radius $R_o$, and there was no damping term included in the analysis. This departure from the true cavity response was brought about by the assumption of isentropic compression and expansion of the air inside the cavity and the neglect of compressibility effects in the fluid outside the cavity. However, valuable information can be gained concerning the frequency and peak pressures associated with the cavity's repeated expansion and collapse. To aid in the study of these parameters, the computer output was designed to reflect the cavity pressure fluctuations with time. This was accomplished by plotting the output in the following form: cavity pressure/ambient fluid pressure versus time. This

pressure is directly related to the cavity radius as shown by equation (6). An example of the output, which was computed for an initial pressure ratio of 6.67, is shown in Fig. 8. This plot illustrates the cavity pressure oscillation with time, and further it predicts that the peak pressure occurs when the cavity is at its minimum radius. This fact has been shown experimentally by Cole (Ref. 1).

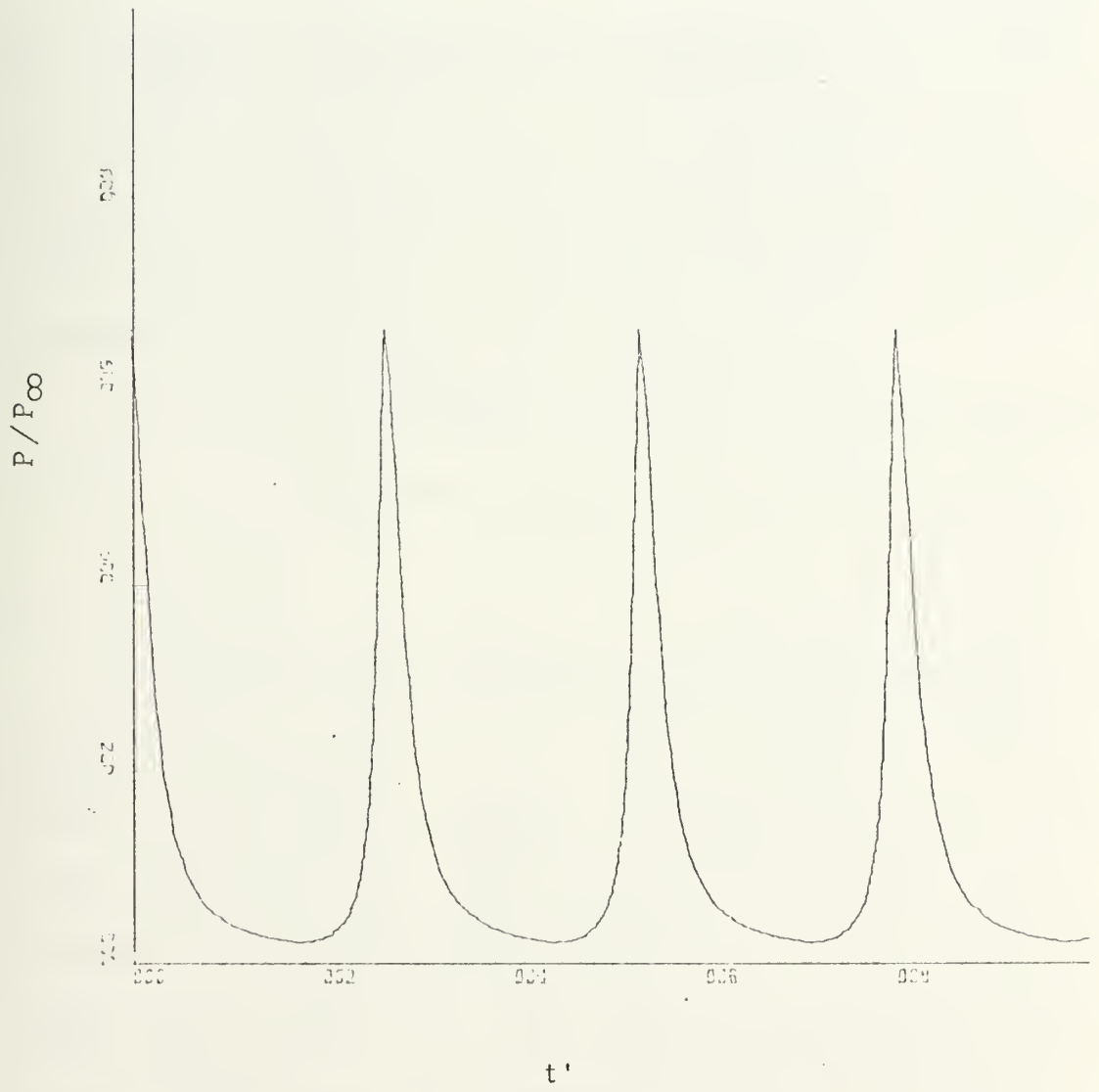


Fig. 8 Hydraulic Ram Cavity Pressure Oscillation.

## IV. APPARATUS

The test apparatus consisted of projectile accelerators, test specimens, a test tank, and associated instrumentation for evaluating the effect of high-velocity impact into liquid filled containers.

### A. PROJECTILE ACCELERATORS AND PROJECTILES

A 0.22 caliber rifle was used to accelerate the projectiles. The rifle was mounted on a stand, as shown in Fig. 9, and located about 6.9 meters from the target tank. Impact tests were made with projectile velocities in the order of 0.381 km/sec (1250 ft/sec).

The cartridges were factory loaded 0.22 caliber long rifle ammunition with a solid lead projectile weighing 1.95 grams.

### B. TEST TANK

The test tank used for the impact tests was fabricated from transparent plexiglas, Type G, 25.4 millimeters (1 inch) thick. The tank was square in shape, with the plexiglas making up the top, bottom, and two sides. The front and rear of the tank had removable and replaceable walls into which impact was made. A photograph of the tank with its support table is shown in Fig. 10. In this investigation, the removable walls were made from 7075-T6 aluminum sheet 1.27 millimeter (0.050) thick, secured to the transparent walls by a clamping frame.

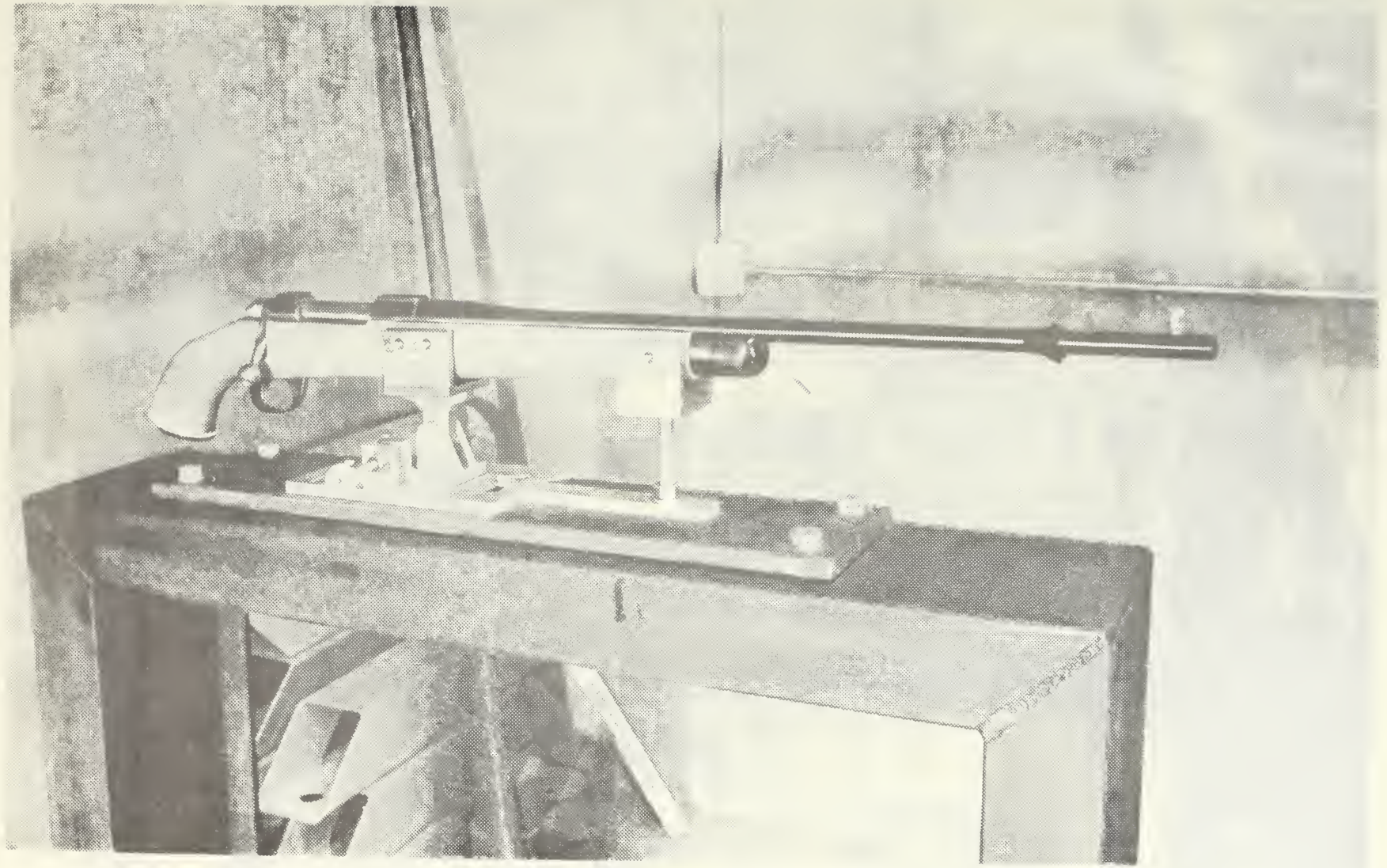

Fig. 9 Ballistic Range Rifle Mount

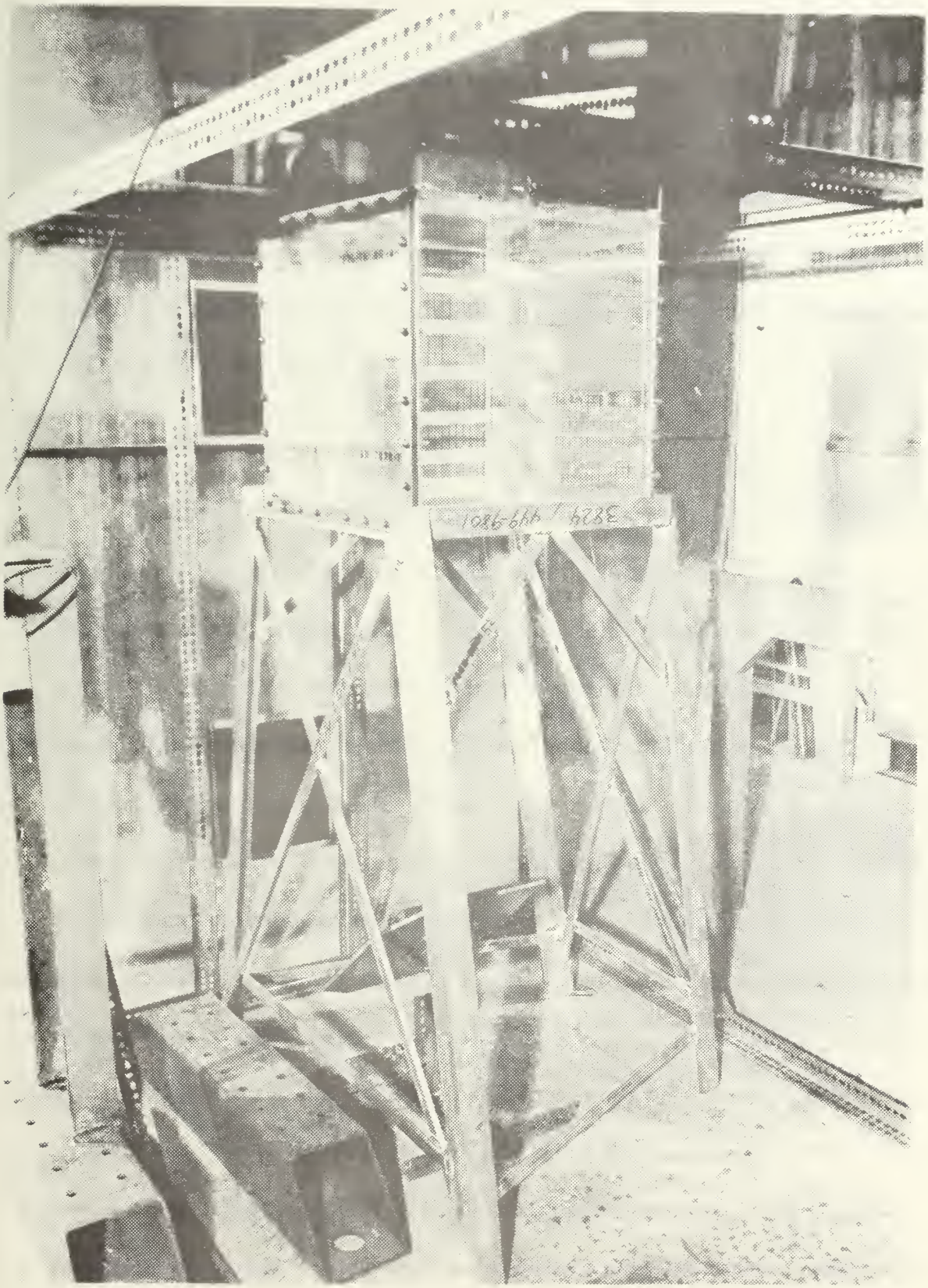

Fig. 10 Test Tank Installation.

## C. RANGE LAYOUT

The basic elements of the ballistic range are shown in schematic form in Fig. 11. The down-range photograph (Fig. 12) shows the velocity sensors and the three shadowgraph stations located along the flight path. These shadowgraph stations were used in conjunction with the velocity sensors to accurately determine the velocity and attitude of the projectile passing down the range.

## D. INSTRUMENTATION

The projectile was a chronograph screen with a 5-volt d.c. potential across it. When the screen was broken by a projectile, a pulse was sent through a signal conditioner, then to the delay unit, and finally to a counter. Two Monsanto 101B counters were used for velocity measurement. The delay units were used to trigger the shadowgraph spark sources at the proper time. Figure 13 shows the circuitry of the two delay units used in timing the dual shadowgraph system of the test tank. The major component of each delay unit was a Signetics N74123 retriggerable monostable multivibrator. These units generate variable time delays from 200 $\mu s$ to 1700 $\mu s$ and from 3 $\mu s$ to 18 $\mu s$, respectively. A spark source triggering capacitor was built into each delay unit. The signal conditioner, shown in Fig. 13, was needed to compensate for the wide range of resistances found in the chronograph screens. The signal conditioner was basically a transistor switch using a 2N3404 transistor.

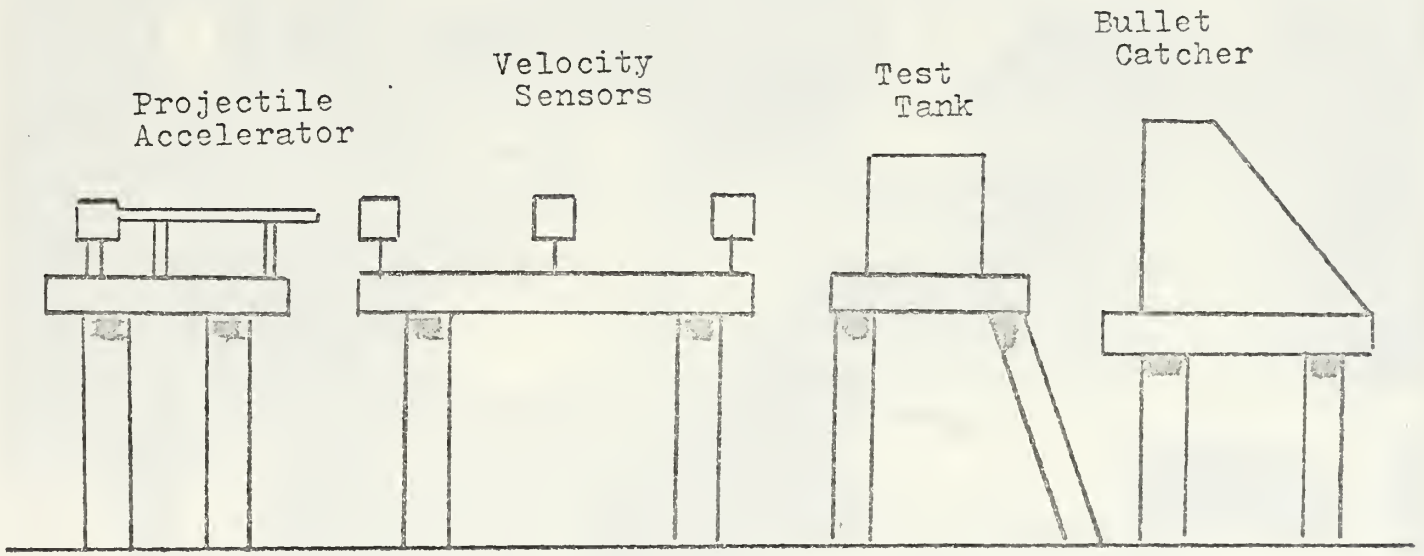


Fig. 11 Ballistic Range Layout.

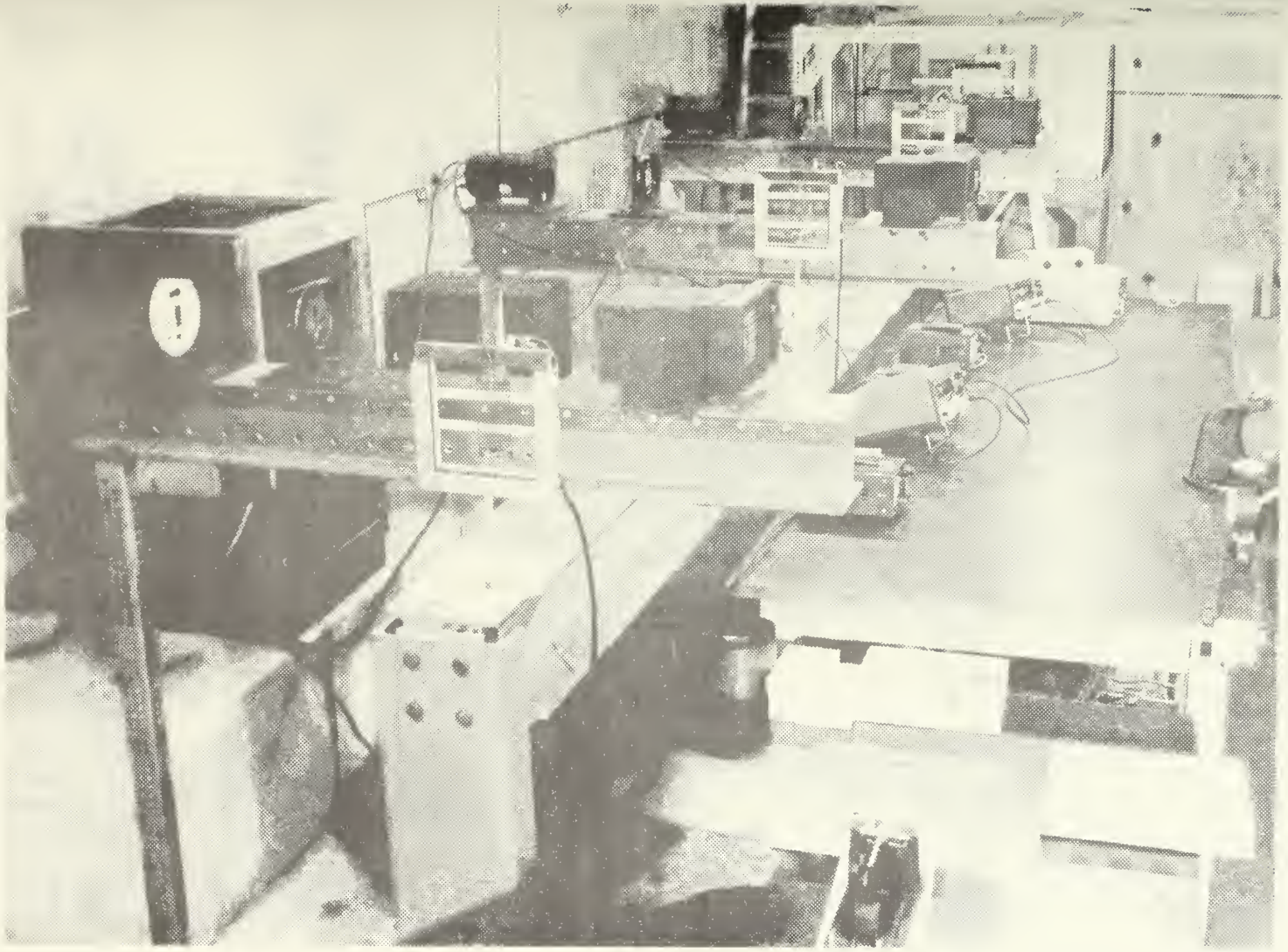

Fig. 12 Ballistic Range Configuration (Down-range View)

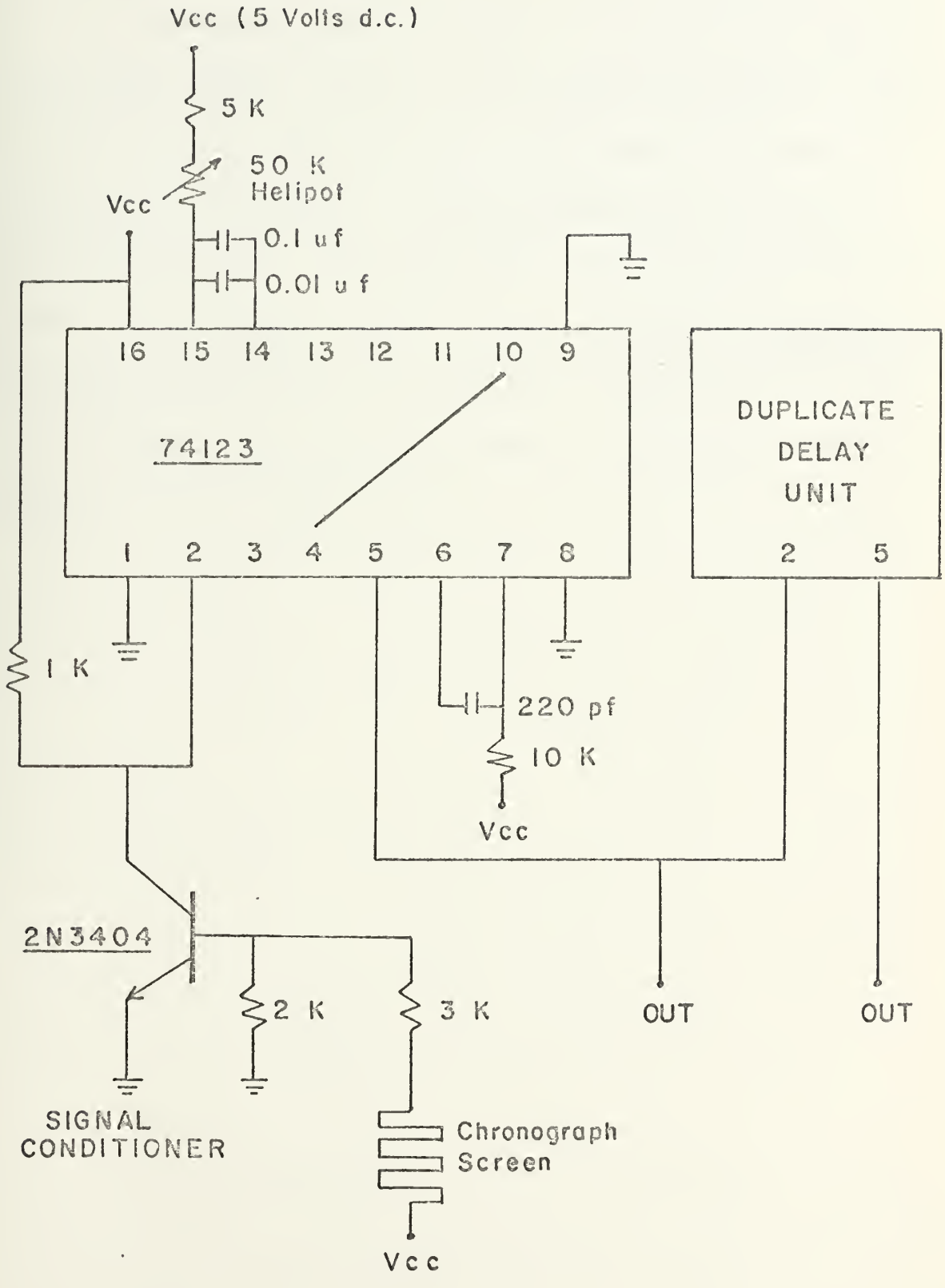


Fig. 13 Delay Unit Circuitry.

## E. SHADOWGRAPH SYSTEM

The shadowgraph system associated with the test tank consisted of two similar stations. Figure 14 is a schematic representation of the apparatus showing a down-range view. Each shadowgraph station was composed of a spark source, a 16-inch collimating mirror, and a 4- x 5-inch photographic plate. The spark source was located at the focal point of the mirror to provide the necessary collimated light. Polaroid Type 57 high-speed film was used to record the shadowgraphs through the water filled test tank. The complete shadowgraph system is shown in Figs. 15 and 16.

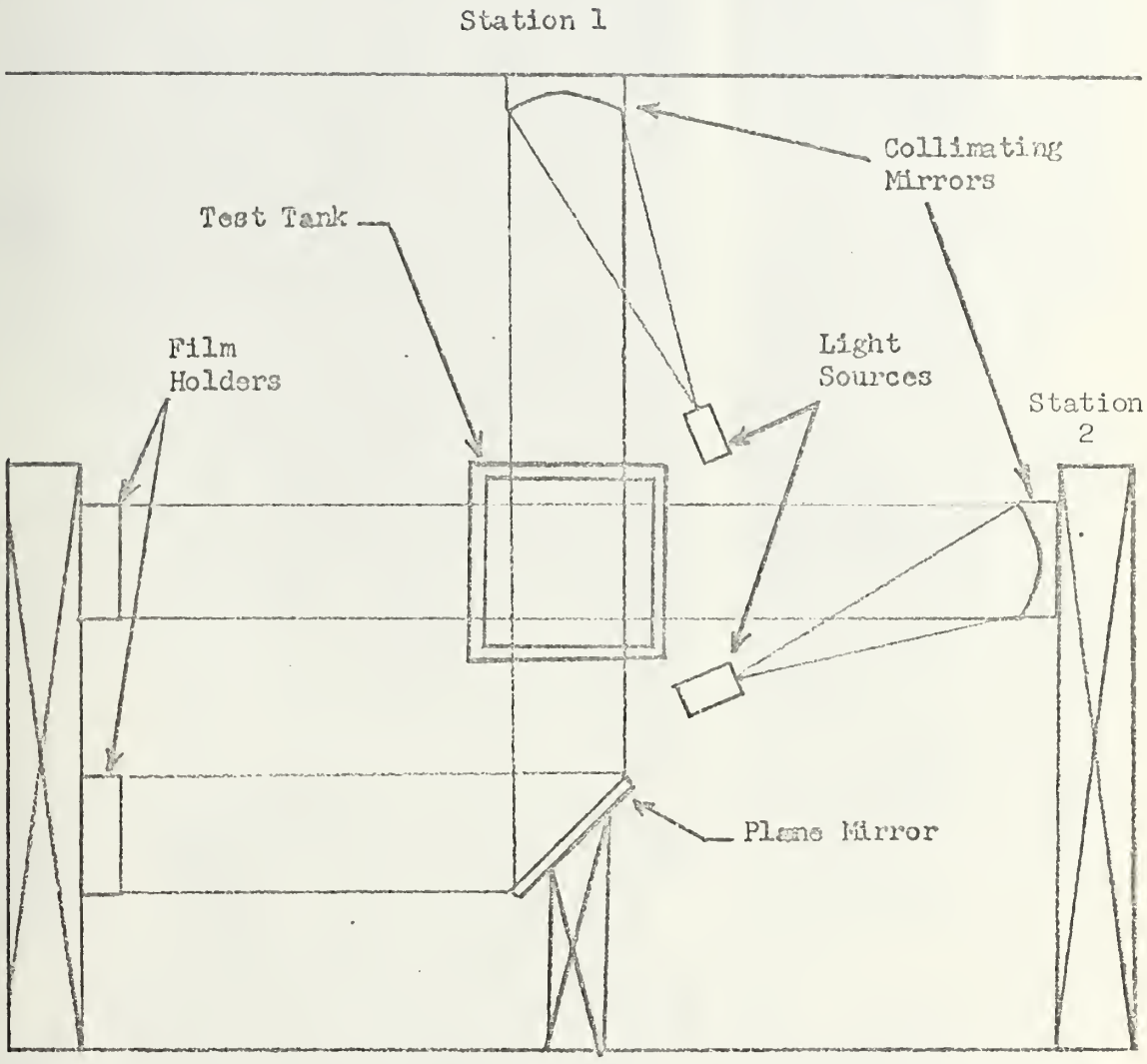


Fig. 14 Schematic of Shadowgraph Apparatus (Down- range View).

Fig. 15 Dual Shadowgraph System (Test Tank and Collimating Mirrors).

Fig. 16 Dual Shadowgraph System
(Plane Mirror and Film Holders).

## V. RESULTS AND DISCUSSION

This research was conducted as a preliminary investigation of the mechanisms involved in hydraulic ram. Primarily, the phenomena studied were the characteristics of the shock wave pressure pulse generated in water from impact by a projectile and the rate of energy loss of the projectile in the water. By the characteristics of the shock wave pressure pulse one means the shape and progress of the shock wave with time and the magnitude of the pressures at the wave front.

### A. SHAPE OF THE SHOCK WAVE FRONT

The investigation of Ref. 3 indicated that the shape of the pressure wave front generated in the water by a projectile impact was hemispherical. However, the data of this reference were primarily limited to impacts with spherical projectiles. Since the typical threat to an aircraft fuel tank has the standard bullet shape, the projectiles used in the investigation were solid lead bullets. The influence of lead bullets, which deform as they enter the tank and traverse the fluid, was explored and will be discussed in a later section of this report.

The shape and propagation of the pressure wave front resulting from the projectile impact were obtained from the dual high-speed shadowgraphs. A typical dual shadowgraph sequence of the pressure wave front progress is shown in Fig. 17. The figure illustrates the results of the impact by a 1.95 gram lead bullet at a velocity of 0.374 kilometers per second

(1226 ft/sec) into water in the transparent plexiglas test tank. For this test the projectile passed through a 0.5-inch diameter, "pre-punched" hole in the entry wall. A strip of masking tape was used to cover the hole and contain the water. A hemispherical wave front was produced, and the center of the hemisphere remained at the point of impact as the wave front expanded. The photographs of Fig. 17 show that there was no significant effect of the forward momentum of the projectile to move the wave front in the direction of flight.

A commonly used model for analytical prediction of the hemispherical wave strength and motion is the blast wave theory. Blast wave theory assumes sudden release of energy centered at the projectile penetration point. The behavior of the fluid properties as a function of radius will not be consistent with that model. See, for example, Chapter 4 of Sedov (Ref. 11).

An alternate and more accurate model would be to assume an expanding hemispherical piston due to projectile penetration. The rate of change of piston radius $r_p$ would be

$$\frac{\partial r_p}{\partial t} = \left[\frac{3}{2\pi}\frac{\partial V}{\partial t}\right]^{1/3} \tag{10}$$

The quantity $\partial V/\partial t$ equals the rate at which the projectile displaces fluid volume during penetration.

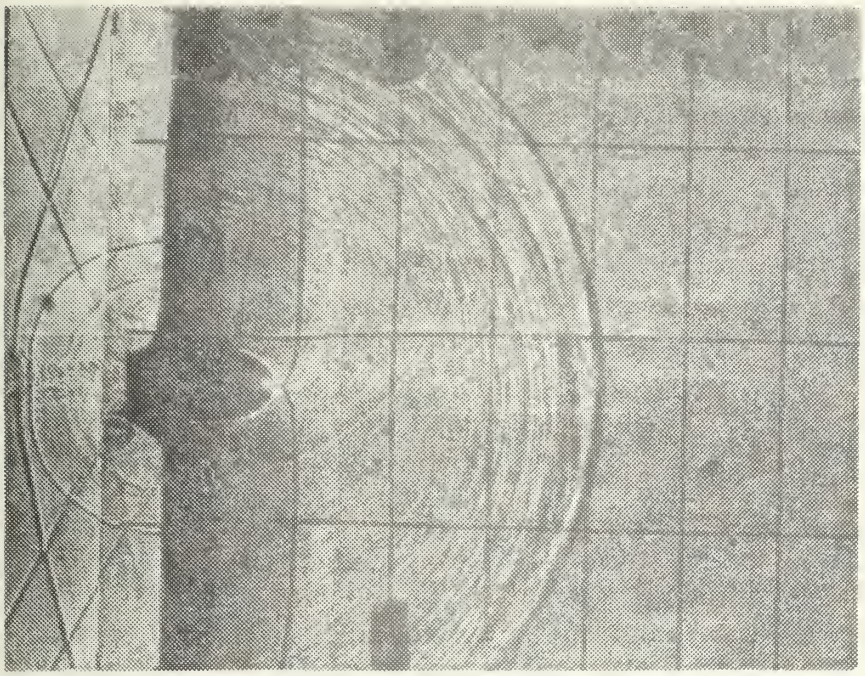

27 μs after impact

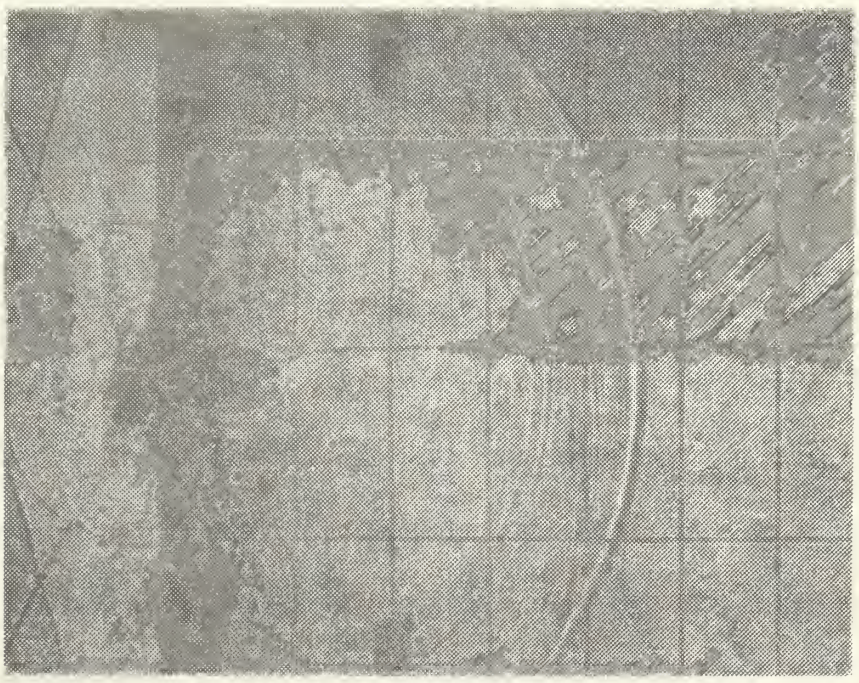

32 μs after impact

Fig. 17 Shock Waves Resulting from a Pre-punched Wall Impact.

Tests were also performed with a solid front wall on the test tank. The entry walls used were 7075 - T6 aluminum sheet 1.27 millimeter (0.050 in.) thick. An example of the resulting wave front due to solid wall penetration is shown in Fig. 18. This set of photographs illustrates the obscuration of the interior of the shock wave due to the projectile penetration of the entry wall. The shadowgraphs show that the hemispherical wave front was produced as in the "pre-punched wall case." The other wave front in the water, which appears as a straight line oblique to the wall, was caused by the propagation of shear and dilatation waves (Ref. 12) moving through the metal at a faster rate than the waves through the water. The rate of propagation of this oblique wave was found to be proportional to the bulk sonic velocity (dilatation wave) for aluminum (6.2 km/sec).

## B. PROGRESS OF THE SHOCK WAVE WITH TIME

Impacts with projectiles of various kinetic energies were made to determine the influence of kinetic energy on shock wave velocity. The average velocities of the shock waves were determined from shadowgraphs similar to those in Figs. 17 and 18. The shadowgraphs were used to obtain time and position information for the shock wave as it expanded and propagated through the fluid. The slopes of the resulting time - distance plots supplied the average propagation velocities of the shock waves.

Figure 19 is a plot of the resulting shock front velocities for an impact kinetic energy of 135.2 joules. This plot shows that the shock front velocity decays to the acoustic speed in water by a distance

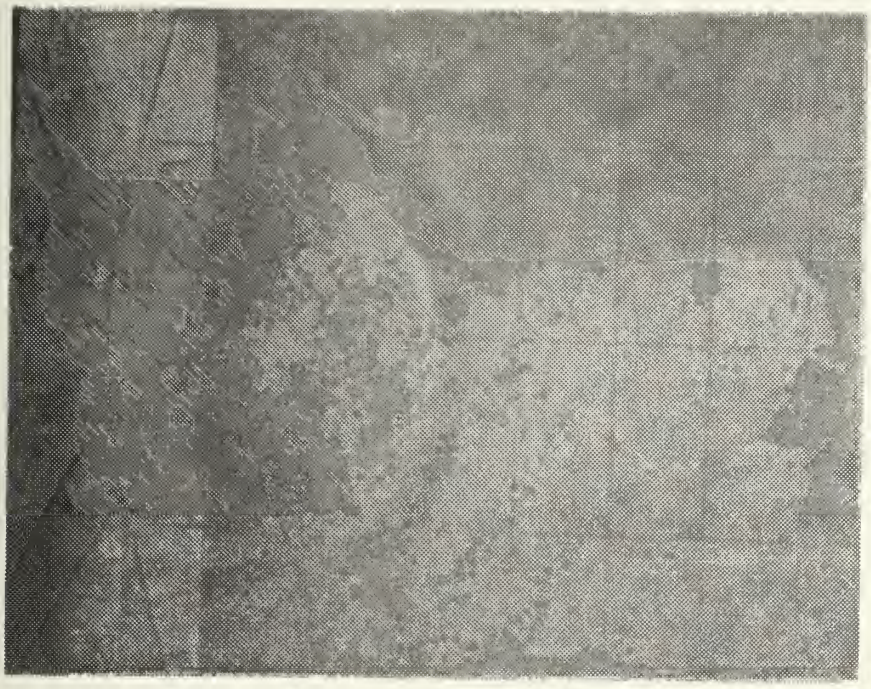

18 $\mu s$ after impact

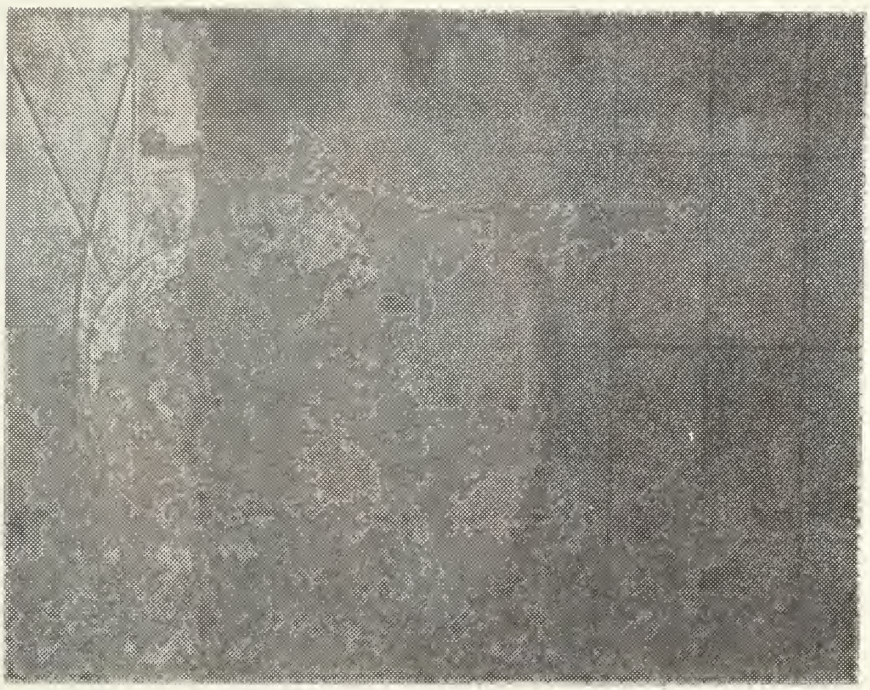

25 $\mu s$ after impact

Fig. 18 Shock Waves Resulting from a Solid Wall Impact.

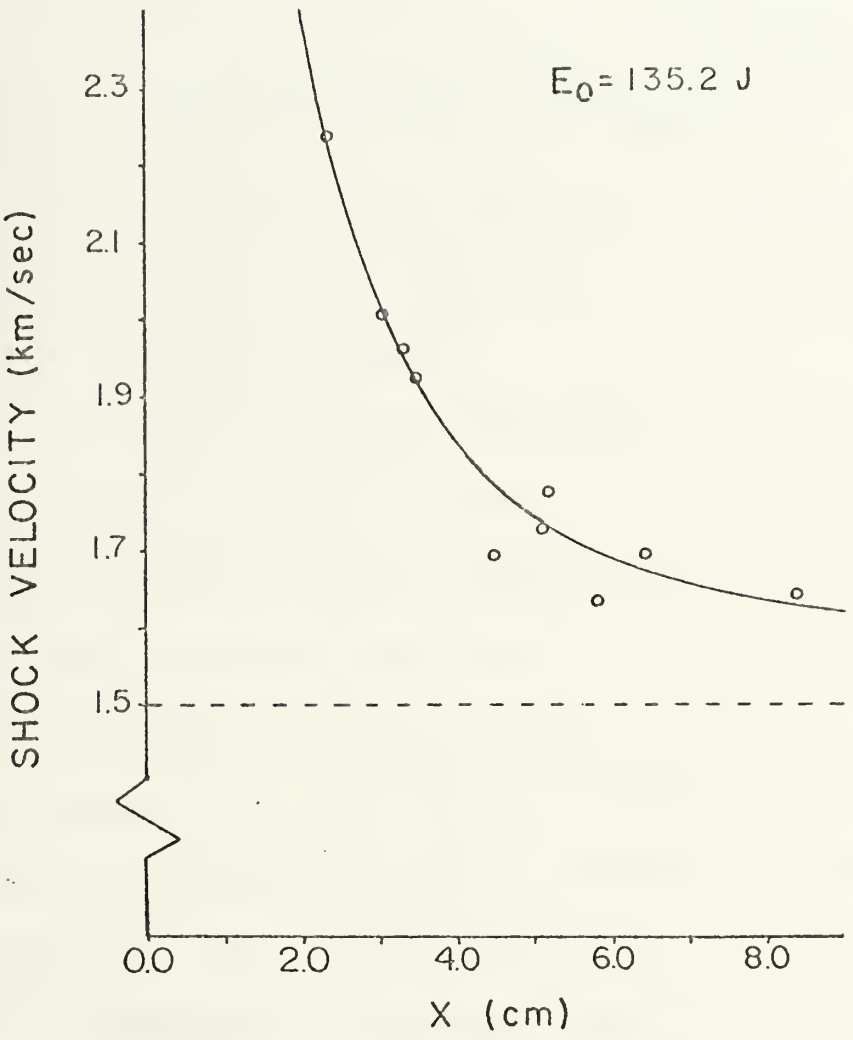


Fig. 19 Shock Front Velocity Generated in Water by Projectile Impact.

of about 11 centimeters (4.3 in.) for this impact energy. The acoustic speed for water used in this investigation was 1.5 kilometers per second (4920 ft/sec).

## C. PRESSURES GENERATED IN THE FLUID

The pressure generated in the fluid by the projectile was divided into two regions. The first region consisted of the pressure associated with the shock front propagation and was considered as the shock phase of the hydraulic ram phenomenon. The second pressure region was concentrated in the immediate vicinity of the projectile itself.

### 1. Shock Front Pressure

Pressures generated in the water at the shock front correspond to the measured shock front velocities and were determined from data given in Table 2.2 in Ref. 1. Figure 20 shows the pressures generated at the shock front corresponding to the data given in Fig. 19 of this report. The result shows that extremely high pressures are generated in the water near the impact point. For example, impact with a 1.95 gram bullet at an impact velocity of 0.372 kilometers per second (1222 ft/sec) resulted in a pressure of 3750 kilograms per square centimeter ( 53,335 lb/sq in.) at a distance of 2.24 centimeters (0.88 in.) from the impact point. These pressures decay rapidly due to geometric expansion of the shock front and, as in the case of the shock velocity, reach ambient values in a short distance.

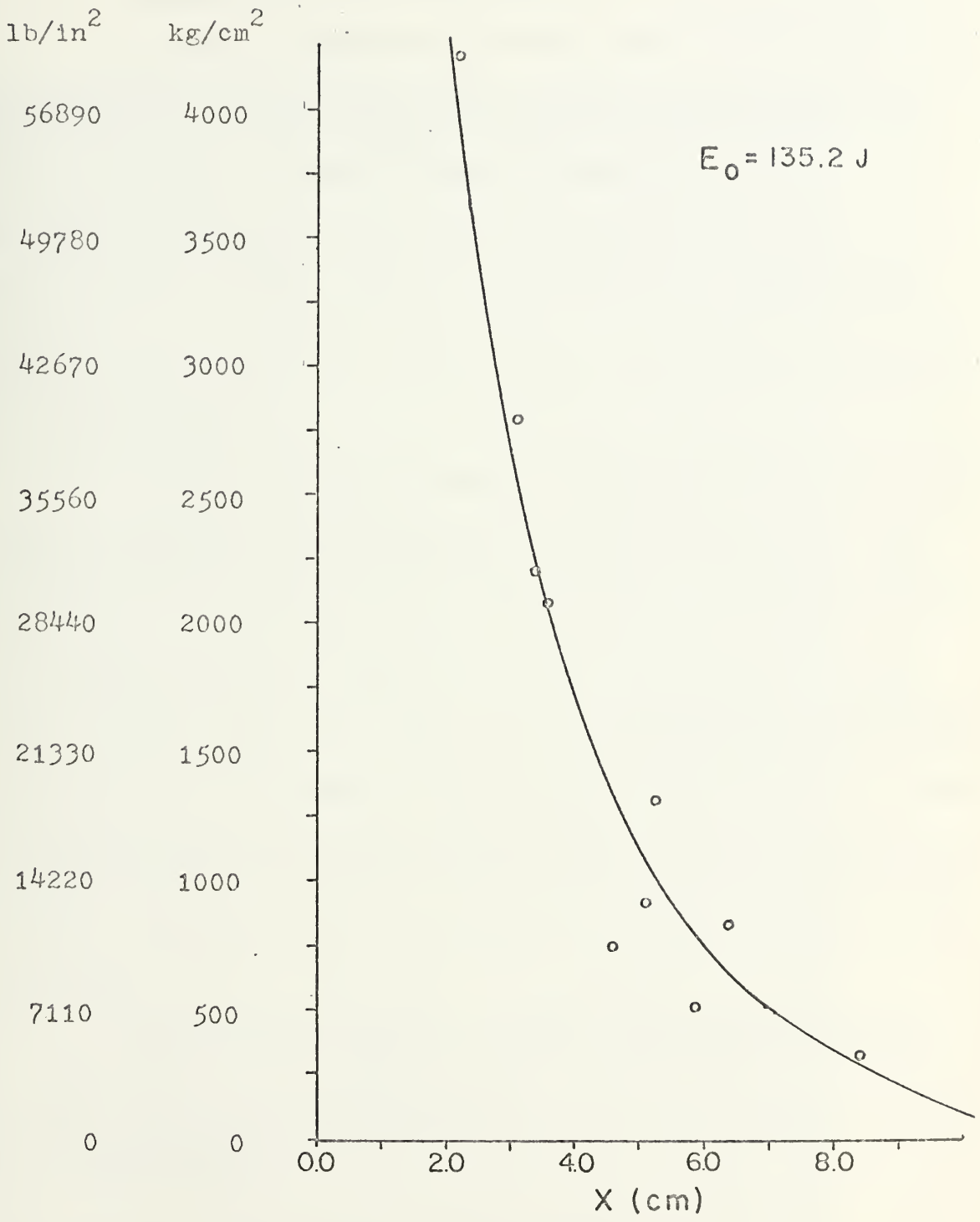


Fig. 20 Shock Front Pressure Generated in Water by Projectile Impact.

2. Pressure Field Around the Projectile

As with any object moving through a fluid, the projectiles created a dynamic pressure in the water due to the stagnation conditions on their front surface. Dynamic pressure is related to the density of the fluid and the square of projectile velocity. For the velocities of 0.372 kilometers per second used in this research, pressures of 710 kilograms per square centimeter ($1.01 \times 10^4$ lb/in$^2$) were found to exist in the vicinity of the projectile.

Further insight into the pressure field around the projectile was gained by examining the light diffraction patterns illustrated in Fig. 21. The concentration of light at the front surface of the projectile was caused by a change in the refractive index of the fluid due to the large increase of pressure and density in this region. Light is refracted toward the larger refractive index which accompanies higher density and pressure in the fluid. A qualitative analysis of the entire pressure field around the projectile can be made by studying the amount and direction of deflection of the grid lines in this area.

Figure 21 also shows the air filled conical cavity behind the projectile. This cavity is a result of the dynamic pressure produced in the fluid by the projectile.

D. PROJECTILE ENERGY DECAY AFTER IMPACT

Measurements were made of the progress of the projectile through the water after impact. From these measurements the projectile velocity and energy loss were determined.

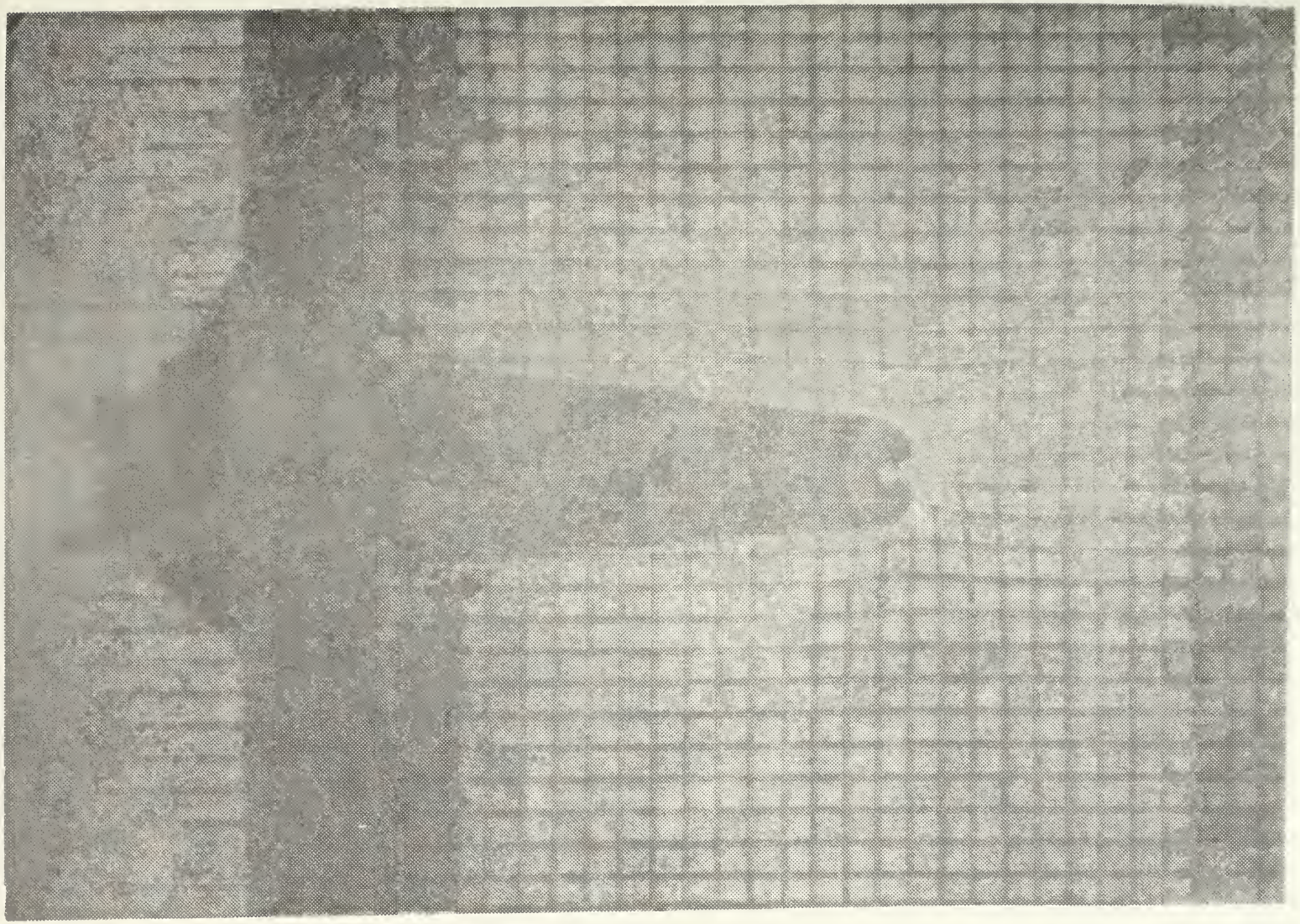

Fig. 21 Light Diffraction Pattern Around the Projectile.

One set of the shadowgraphs from which the projectile velocities were calculated is shown in Fig. 22. These experimentally derived velocities and energies are plotted as a fraction of their impact magnitude versus distance into the tank, as shown in Figs. 23 and 24.

A detailed analysis of the velocity decay or energy loss of a projectile traversing a fluid would be extremely difficult because of the many variable parameters. Assumptions must be made to account for the changes in the projectile's shape, drag coefficient, and material properties. Because of these difficulties, a simplified analysis of the projectile velocity and energy loss was made and compared with the experimental data.

The following drag equation was used:

$$D = -m\frac{dV}{dt} = \frac{1}{2}\rho_f V^2 C_D A \tag{11}$$

Rearranging terms, knowing $V = dx/dt$, gives

$$-\frac{dV}{V} = \frac{\rho_f C_D A\, dx}{2m} \tag{12}$$

Assuming a constant deformed projectile area of 0.5 square centimeters, constant drag coefficient of 1.0, and constant projectile mass, integration yields:

$$\frac{V}{V_o} = e^{-\frac{\rho_f C_D A x}{2m}} \tag{13}$$

Squaring both sides of this relation gives the ratio of the projectile energy after impact to the projectile impact energy. These calculated ratios for the projectile velocity and energy are compared with the experimental data

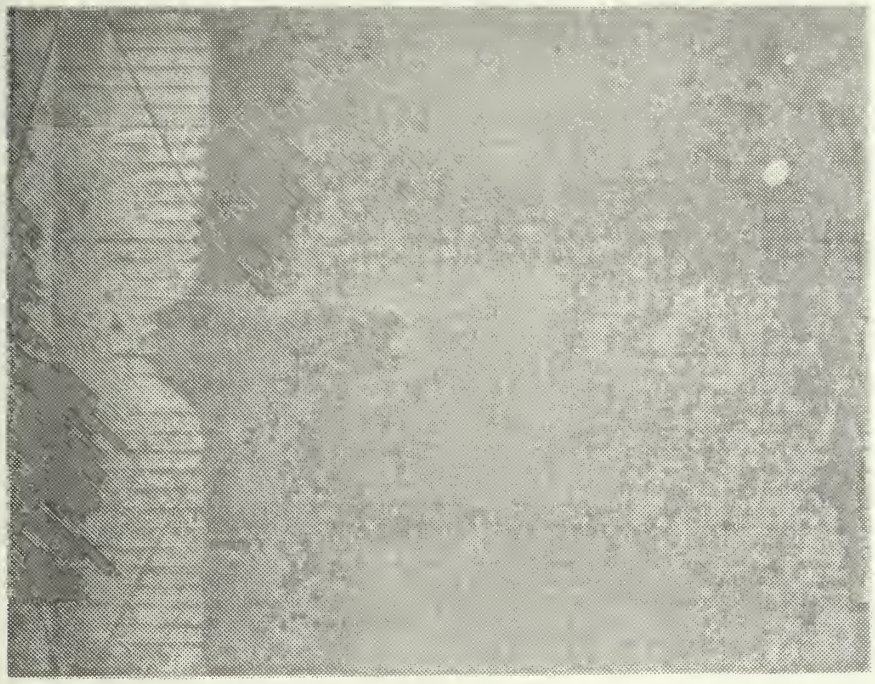

100 $\mu s$ after impact

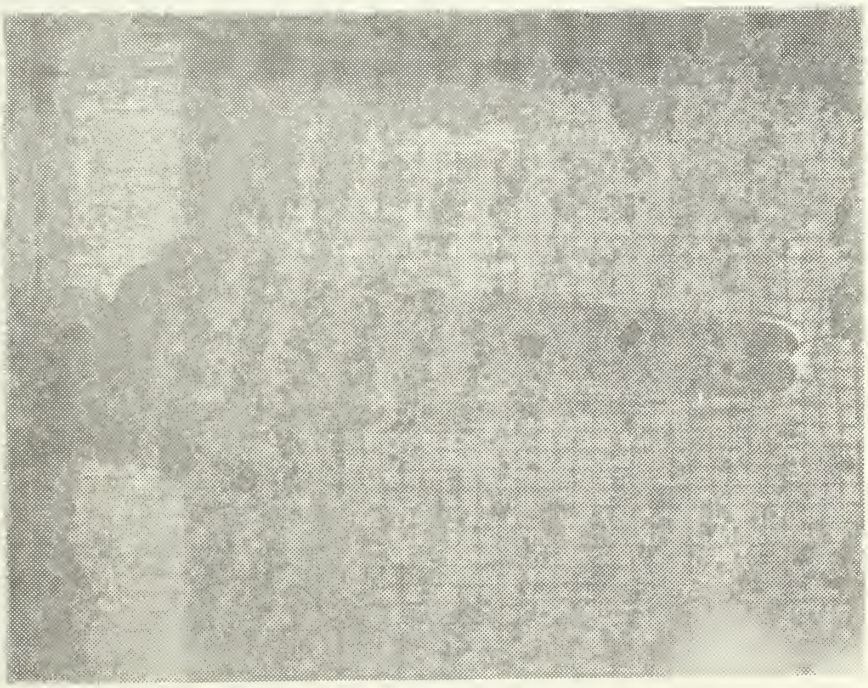

264 $\mu s$ after impact

Fig. 22 Projectile Progress into the Tank.

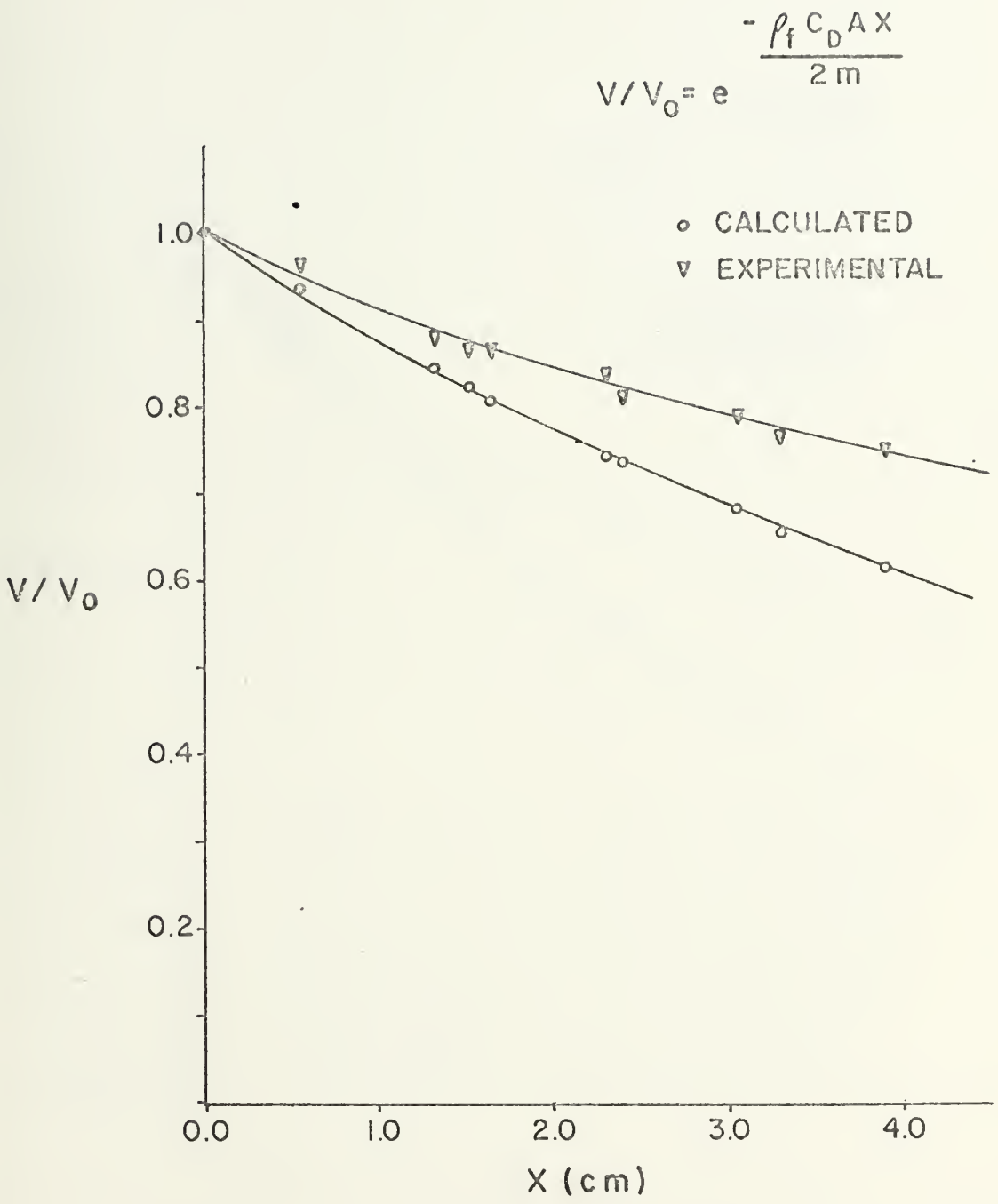


Fig. 23 Projectile Velocity Decay Ratio as a Function of Distance into Tank.

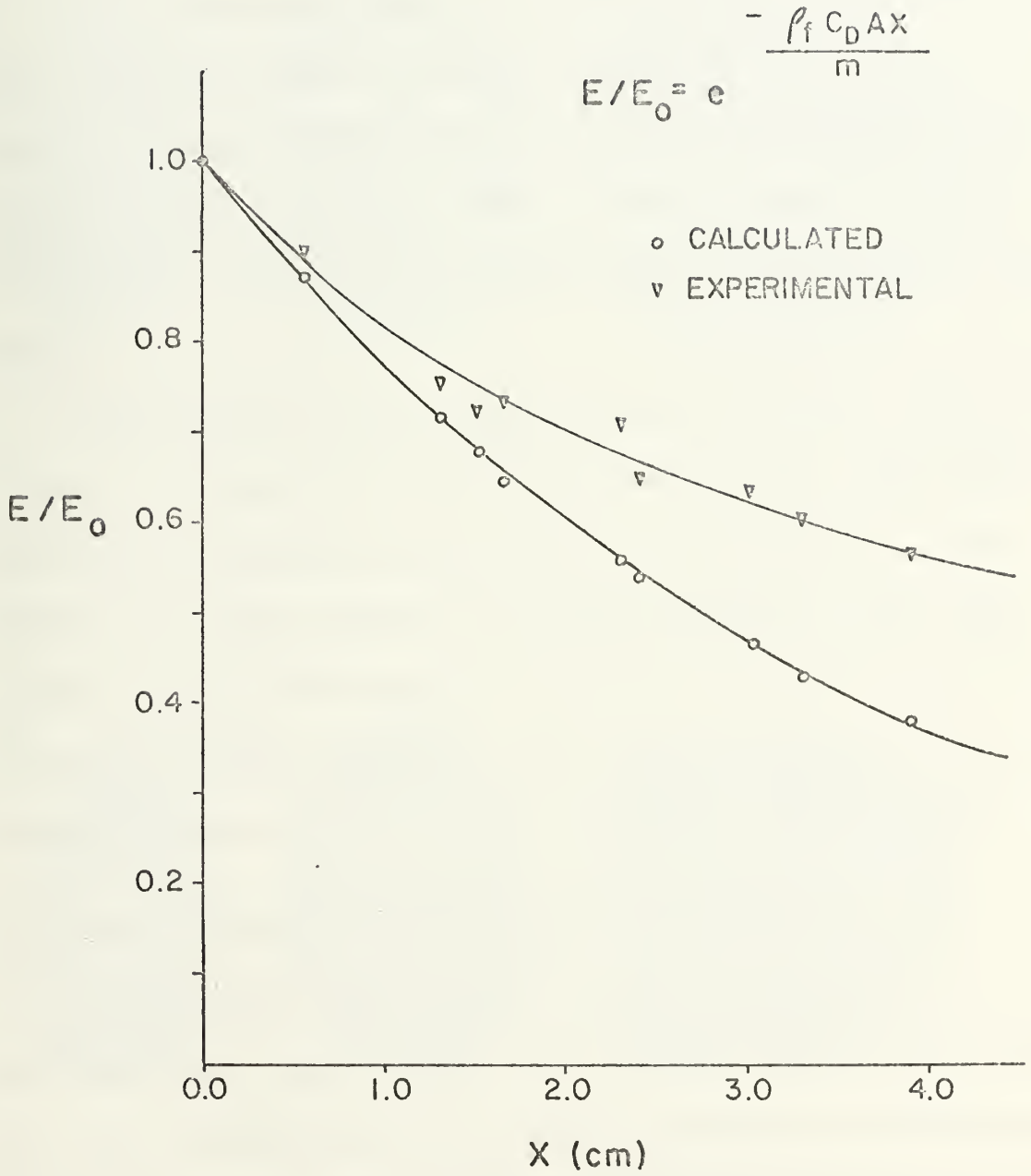


Fig. 24 Experimental and Calculated Ratios of Projectile Energy.

in Figs. 23 and 24. This comparison indicates that in spite of the simplifying assumptions, the agreement between the calculated and experimental values of the velocity and energy after impact was fairly good.

In the experimental tests, the actual projectiles underwent a continual deformation during deceleration in the tank. An increase in frontal area accompanied the deformation, resulting in an average final projectile area of 0.5 square centimeters. This was the area used in the calculated approximation of the velocity and energy decay and constitutes the major cause for error.

Energy decay of the projectile can be directly related to the amount of energy being transferred to the fluid by the projectile. More importantly, the slope of the projectile energy decay curve gives the rate of energy transfer to the fluid, assuming no projectile deformation. This energy transfer rate has been established as a major factor in determining the severity of hydraulic ram (Ref. 7). The average energy transfer rate for the projectiles tested was 20.6 joules per centimeter of fluid traversed.

## E. PROJECTILE DEFORMATION AFTER IMPACT IN FLUID

The projectiles were recovered after each experimental test and were found to display a unique pattern of deformation. The deformation phenomenon was very consistent for the projectiles impacting the fluid through the pre-punched plates. Three examples of projectiles after this type of impact are shown in Fig. 25. The extent of deformation was found to vary directly with the impact velocity; however, all of the projectiles exhibited an identical pattern of having one flat side and one undeformed side. This pattern

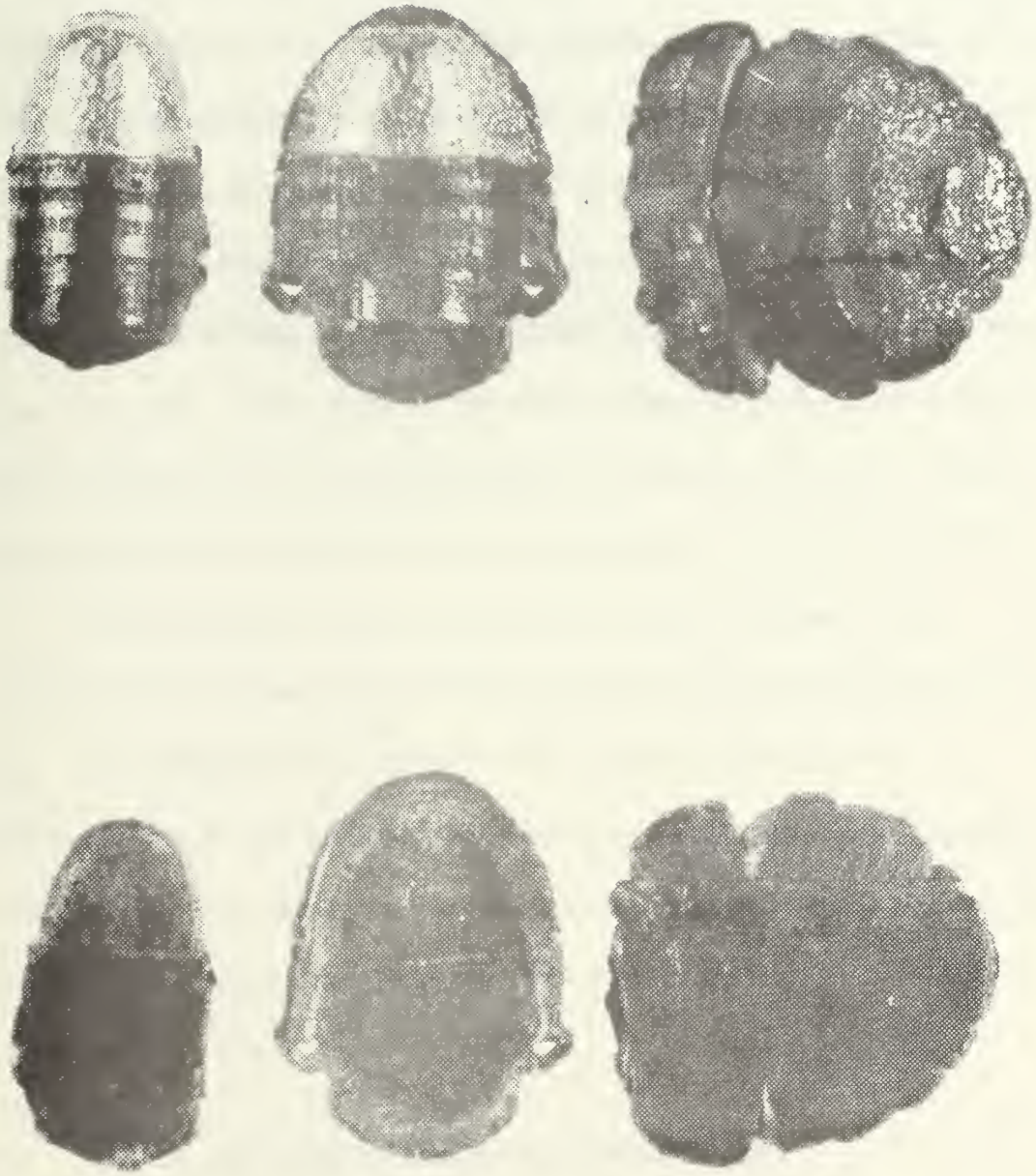

Fig. 25 Projectiles After Impact Through
Pre-punched Entry Wall

of deformation suggests a positive dynamic stability for the projectiles as they traverse the fluid after impact. Once initially flattened, the projectile maintains a fixed attitude due to its stability, and all further deformation takes place on the same flattened side. As shown in Fig. 26A, the dynamic stability of the projectile is maintained through an equilibrium condition between the pressure force, located at the center of pressure, and the inertia force, acting through the center of gravity of the projectile. Figure 26B demonstrates the effect of displacing the projectile from the equilibrium position. The center of pressure moves upward on the slightly curved front surface of the projectile with the stagnation point; this creates a restoring moment which returns the projectile to the stable position.

The projectiles which penetrated a solid entry wall before traversing the fluid did not demonstrate the previously discussed deformation phenomenon. Two typical projectiles of this type are shown in Fig. 27. The small aluminum cap located above each projectile in the photograph is the piece of the entry wall punched out by the projectile as it passed through the aluminum plate. A photograph of an entry wall after a test shot is shown as Fig. 28.

## F. SHOCK AND CAVITY PHASE SEPARATION POINT

When the projectile first penetrates the wall, a strong shock wave pressure pulse is created. As shown in Fig. 29, this pressure decays in strength as it progresses outward. At time $t_A$ in Fig. 29 the pressure behind the shock greatly exceeds the stagnation pressure on the projectile

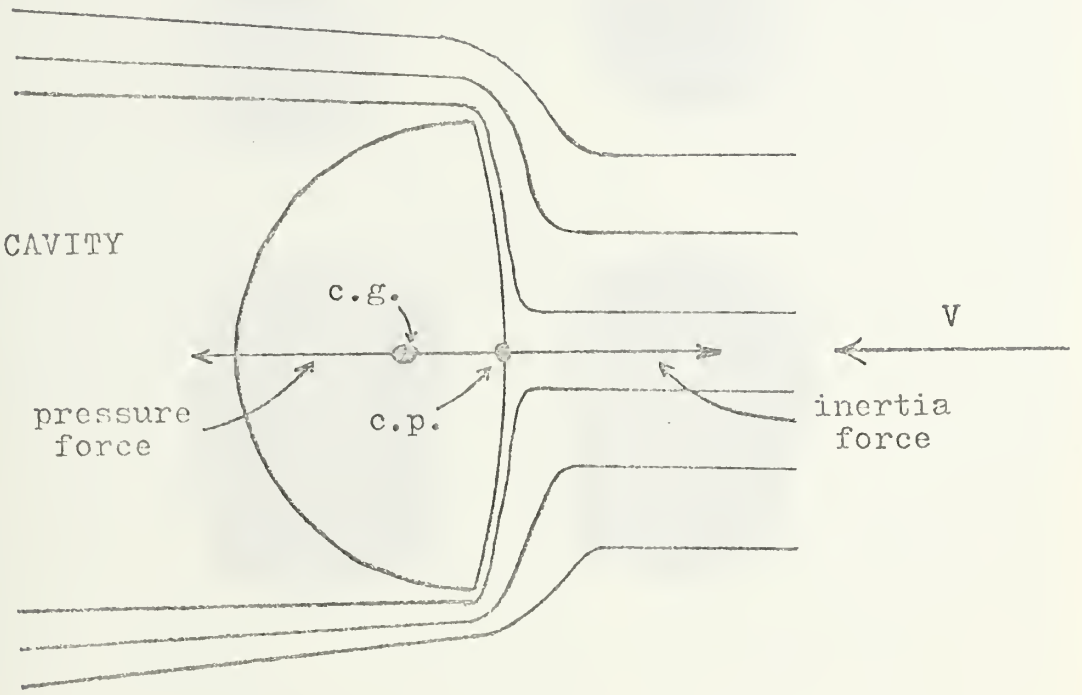


(A) At equilibrium

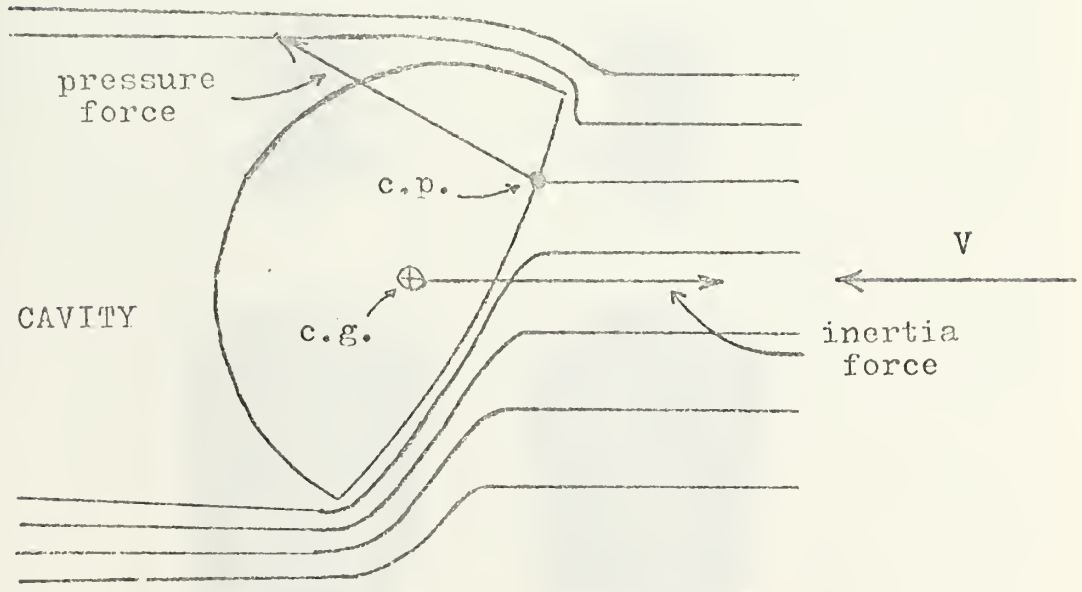


(B) Displaced from equilibrium

Fig. 26 Dynamic Stability of a Deformed Projectile in Water After Impact.

Fig. 27 Projectiles After Impact Through Solid Entry Wall.

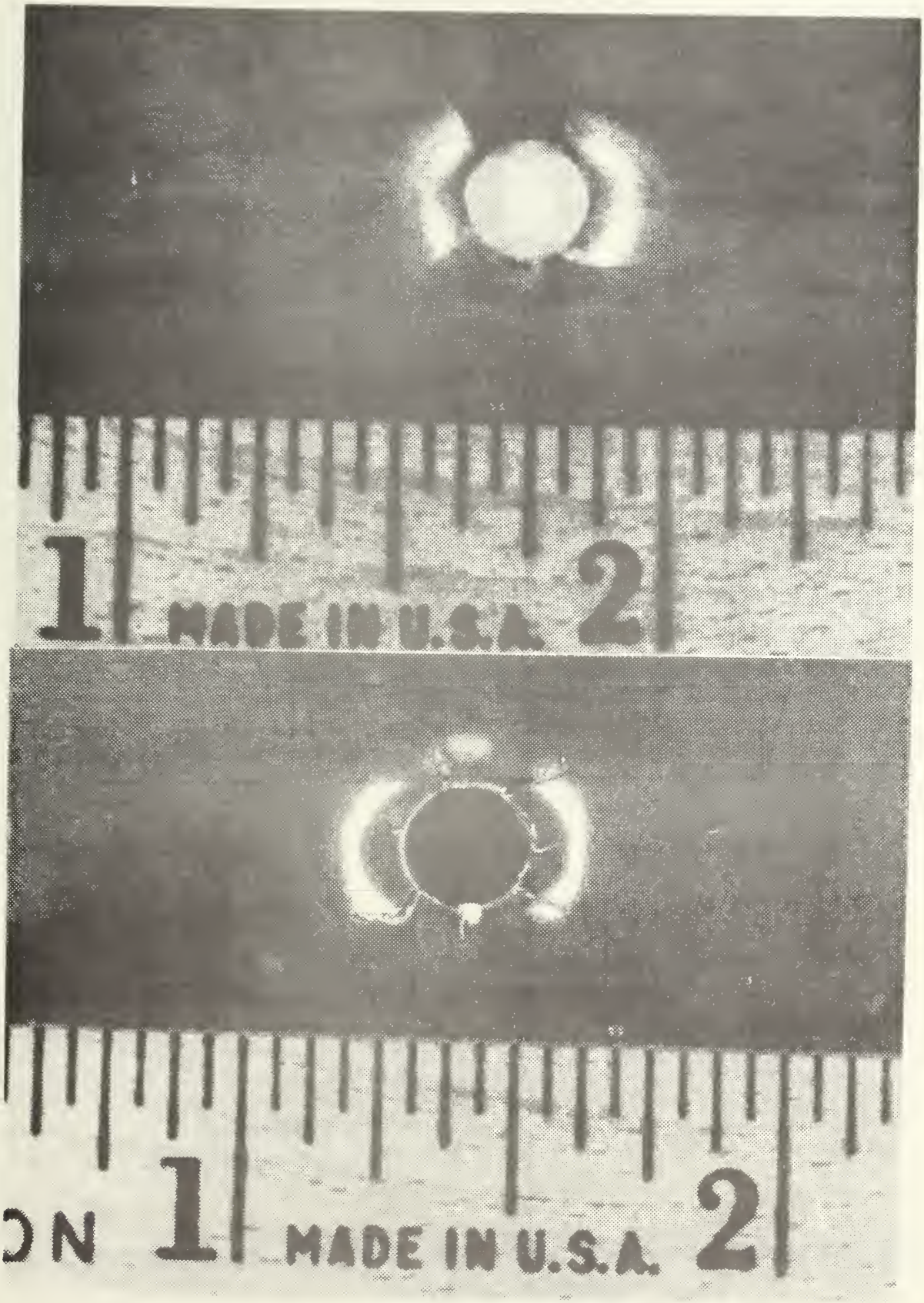


Fig. 28 Solid Entry Wall After Impact.

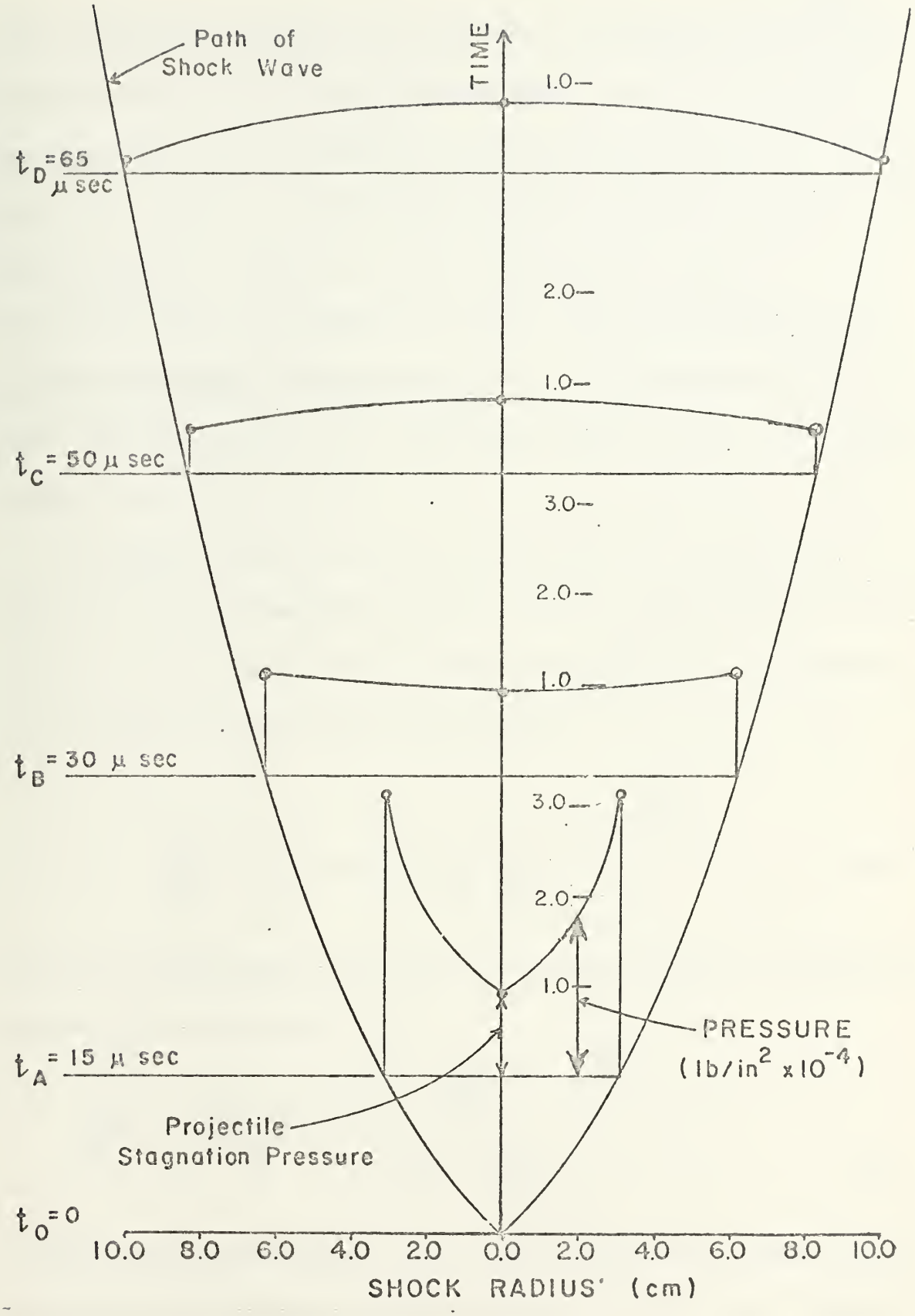


Fig. 29 Evolution of Pressure in the Transition from Shock to Cavity Phase.

nose. Comparing pressures at $t_A$ and $t_B$, it is apparent that both the pressure behind the shock and at the projectile forward stagnation point are decaying; however, the decay of the pressure behind the shock is much more rapid. At time $t_C$ the stagnation pressure exceeds the pressure behind the shock wave. Therefore, at some point between $t_B$ and $t_C$ the two pressures, shock and stagnation, are equal. One could define this as a characteristic time separating the shock and cavity phases of hydraulic ram. The characteristic time for the impact energy of 135.2 joules shown in Fig. 29 is 32 microseconds.

A comparison can be made to further understand the differences between the shock wave and projectile pressures. The stagnation pressure created on the nose of the projectile as it passes through the fluid can be modeled by steady flow and the equation (14) from Ref. 13,

$$\frac{P_o}{P} = \left[ 1 + \frac{\gamma - 1}{2} \left( \frac{V}{C_o} \right)^2 \right]^{\frac{\gamma}{\gamma - 1}} \qquad (14)$$

while the discontinuity of the shock wave requires the use of the following unsteady flow equation (Ref. 13).

$$\frac{V_s}{C_o} = \frac{(P_{21} - 1)}{\gamma} \left\{ \frac{\frac{2\gamma}{\gamma + 1}}{P_{21} + \frac{\gamma - 1}{\gamma + 1}} \right\}^{1/2} \qquad (15)$$

For the same fluid velocity ($V / c_o = 0.5$) the pressure increase is 19 per cent for steady flow and 84 per cent for unsteady flow. This comparison

explains the large initial pressures of the shock wave as well as their rapid decay since unsteady flow is transitory.

## VI. ALTERNATE APPROACHES TO THE PROBLEM

As a result of the work reported here, the following apparatus and test procedure are recommended for use in the future study of the hydraulic ram phenomenon.

### A. HIGH SPEED FRAMING CAMERA

The use of a high speed framing camera would be the optimum way to visually evaluate the hydraulic ram phenomenon. A camera capable of recording 200,000 frames per second would be ideal for further study of the short-lived events which occur. This rate, a frame every 5 microseconds, would supply a complete time-history for the motion of the shock front and projectile through the fluid.

### B. PRESSURE TRANSDUCER

Pressure transducers are essential for the complete analysis of the complex hydraulic ram pressure field and are recommended for use in future work. The pressure distribution is extremely complex due to tank wall reflections and the continued expansions and collapses of the cavity. Recording apparatus for these pressure phenomena require a high frequency response (about 20 kHz for cavity phase and 1 MHz for shock phase) and are very sensitive to location (Ref. 6). However, it is important that this type of direct pressure readout be compared with previously obtained information.

## C. STRAIN GAUGES

After projectile penetration, a bending moment is produced in the entry wall and propagates with the expanding shock wave pressure pulse. Strain gauges would be valuable in determining both the magnitude and propagation speed of the bending moment and its associated pressure wave front.

## D. HYDROGEN BUBBLE DISPLACEMENT

In the cavity phase of hydraulic ram, knowledge of fluid motion within the tank is important. Hydrogen bubble flow visualization techniques are well suited for investigations requiring determination of the velocity field over an extended region of space in a time-dependent flow. This technique could be used with the transparent test tank and high speed framing camera to determine the pressure distribution surrounding the cavity as it expands and collapses.

## E. HOLOGRAPHIC INTERFEROMETRY

In order to study a material under shock loading, it is necessary to measure both the shock transit time and the profile of the transmitted stress wave. Wall displacement information of this type can be obtained most efficiently through the use of holographic interferometry. The shocked specimen's free surface motion measured by this technique could be studied and related to overall fuel tank response to hydraulic ram.

## VII. CONCLUSION

The following conclusions were obtained from the investigation of the shock wave and cavitation effects of the hydraulic ram phenomenon:

A ballistic range and a simulated fuel tank test apparatus have been designed, built, and made successfully operational.

The nonlinear equations describing cavity oscillation and collapse have been programmed and numerical results obtained.

The rapid energy transfer of the shock phase produces piston-like energy release resulting in a hemispherically shaped pressure wave propagating from the point of projectile impact. The hemispherical shape of the shock wave was found to exist for impacts through thin solid metal and pre-punched tank entry walls.

Very high pressures were produced in the fluid as a result of the projectile impact. A pressure of 3750 kilograms per square centimeter ( 53,335 $lb/in^2$ ) at a distance of 2.2 centimeters from the impact point was produced by a 1.95 gram projectile with an impact velocity of 0.375 kilometers per second.

Good agreement was found between simplified analytical predictions and experimental data for energy lost by the projectile as it decelerated in the fluid.

Large dynamic pressures were produced on the projectile as it passed through the fluid. These pressures, in the order of 700 kilograms per square

centimeter ($10^4$ lb/in$^2$), caused substantial deformation of the solid lead projectiles.

A characteristic time was defined which establishes the point of separation between the shock and cavity phases of hydraulic ram. For an impact energy of 135.2 joules the characteristic time was found to be 32 microseconds.

# APPENDIX A

## DERIVATION OF THE EQUATION OF MOTION FOR THE HYDRAULIC RAM CAVITY

From continuity one obtains

$$\frac{\partial}{\partial r}\left(r^2 u\right) = 0$$

which integrates to the form

$$u r^2 = F(t)$$

Since there is potential flow

$$u = \frac{\partial \phi}{\partial r} = \frac{\dot{R} R^2}{r^2}$$

Integration yields

$$\phi(r,t) = -\frac{\dot{R} R^2}{r} + G(t)$$

Differentiating with respect to time gives

$$\frac{\partial \phi}{\partial t} = -\frac{\ddot{R} R^2 + 2 R \dot{R}^2}{r} + \frac{\partial G}{\partial t}$$

For an incompressible fluid the momentum equation in terms of potential functions is

$$\frac{\partial \phi}{\partial t} + \frac{p}{\rho} + \frac{1}{2}\left(\frac{\partial \phi}{\partial r}\right)^2 = C(t)$$

Considering boundary conditions at infinity $\partial G / \partial t = 0$ and $C(t) = \frac{P_{\infty}}{\rho}$. Combining equations leads to

$$\frac{P}{\rho} = \frac{P_{\infty}}{\rho} + \frac{\ddot{R} R^2 + 2R\dot{R}^2}{r} - \frac{\dot{R}^2 R^4}{2r^4}$$

For conditions inside the cavity, $r = R$, and the preceding equation becomes

$$R\ddot{R} + \frac{3}{2}\dot{R}^2 = \frac{P(R,t) - P_{\infty}}{\rho}$$

which is the equation of motion for a cavity.

```
//HCLM1 JCB (0738,1028,AR22),'HCLM'
// EXEC FORTCLGP,REGION.GO=100K
//FORT.SYSIN DD *
C
C
C       CAVITY PROBLEM NUMBER 1
C
C
C   ***********************************************************
C   *                                                         *
C   *                                                         *
C   *   THIS PROBLEM USES THE NUMERICAL INTEGRATION SUB-      *
C   *   ROUTINE QATR TO SOLVE THE NON-LINEAR CAVITY EQUATION  *
C   *   OF MOTION. PROBLEM NUMBER 1 IS DESIGNED TO COMPUTE    *
C   *   THE COLLAPSE TIME OF A SPHERICAL VACUUM FILLED HYD-   *
C   *   RAULIC RAM CAVITY.                                    *
C   *                                                         *
C   *                                                         *
C   ***********************************************************
C
      EXTERNAL FCT
      DIMENSION T(200),XX(200),AUX(200)
      WRITE (6,13)
C
C     THE INITIAL CONDITIONS FOR PRESSURE, DENSITY, AND
C     CAVITY RADIUS ARE DEFINED.
C
      PINF=2500.
      RHO=1.60
      R=1.0
      A=-1.0/((2.0/3.0)*(PINF/RHO))**0.5
C
C     INTEGRATION PARAMETERS FOR SUBROUTINE QATR ARE
C     ASSIGNED.
C
      XL=0.99000000
      XU=0.99000000
      EPS=0.001
      N=100
      NDIM=40
      DO 1 K=1,N
C
      CALL QATR(XL,XU,EPS,NDIM,FCT,Y,IER,AUX)
C
      B=R*A
      T(K)=-B*Y
      XX(K)=XL
      XL=XL-0.01000000
    1 CONTINUE
      XX(1)=1.0000
      XX(100)=0.0000
      DO 2 M=1,100
      WRITE (6,14) M,XX(M),T(M)
    2 CONTINUE
C
C     SOLUTION ARRAY IS PREPARED FOR PLOTTING USING SUB-
C     ROUTINE DRAW.
C
      REAL*8 TITLE(12)
      READ (5,16) TITLE
      REAL LABLE/'    '/
C
      CALL DRAW (100,T,XX,0,0,LABLE,TITLE,0.0,0.0,0,1,0,0,5,
     6,0,LAST)
C
   13 FORMAT ('1',/////,T23,'R/RZERO',T43,'TIME TO CAVITY CO
     LLAPSE')
   14 FORMAT (/,T15,I3,T23,F8.6,T48,F8.6)
   16 FORMAT (6A8)
      STOP
      END
```

```
      FUNCTION FCT(X)
      FCT=X**1.5/(1.0-X**3.0)**0.5
      RETURN
      END
//GO.SYSIN DD *
HOLM,D.  TIME TO CAVITY COLLAPSE FROM RZERO
         TO A RADIUS R (PLOTTED AS R/RZERO)
```

```
//HOLM JOB (0738,1028,AR22),'HOLM',TIME=4
// EXEC FORTCLGP,REGION.GO=100K
//FORT.SYSIN DD *
C
C
C       CAVITY PROBLEM NUMBER 2
C
C
C   ***********************************************************
C   *                                                         *
C   *                                                         *
C   *  THIS PROBLEM USES THE NUMERICAL INTEGRATION SUB-       *
C   *  ROUTINE QATR TO SOLVE THE NON-LINEAR CAVITY EQUATION   *
C   *  OF MOTION. PROBLEM NUMBER 2 IS DESIGNED TO COMPUTE     *
C   *  OSCILLATORY MOTION OF A GAS FILLED HYDRAULIC RAM       *
C   *  CAVITY. THE OUTPUT IS A PLOT OF THE CAVITY PRESSURE    *
C   *  RATIO VS TIME.                                         *
C   *                                                         *
C   *                                                         *
C   ***********************************************************
C
      EXTERNAL FCT,F
      DIMENSION T(500),P(500),AUX(500)
      COMMON GAMMA,ALPHA
      WRITE (6,19)
C
C     THE INITIAL CONDITIONS FOR PRESSURE AND PROPERTIES
C     OF THE GAS ARE DEFINED.
C
      GAMMA=4.0/3.0
      PRATIO=6.667
C
C     'TIME' IS THE CUMULATIVE TIME COUNTER.
C
      TIME=0.0
      ITMAX=50
C
C     N IS THE SOLUTION ARRAY COUNTER.
C
      N=1
C
C     THE FIRST ROOT OF THE CAVITY EQUATION OF MOTION IS
C     FOUND USING SUBROUTINE ZFALSE.
C
    1 XL=0.30
      XR=0.50
      ALPHA=PRATIO/(GAMMA-1.0)
C
      CALL ZFALSE (F,0.001,3,XL,XR,XAPP,ITMAX,IER)
C
      PP=PRATIO
      PROOT=XAPP**(3.0*GAMMA)
      PRATIO=PROOT*PRATIO
C
C     INTEGRATION PARAMETERS FOR SUBROUTINE QATR ARE
C     ASSIGNED.
C
      XLOW=0.999
      XU=0.999
      DO 2 I=N,500
      IF (I.EQ.311) GO TO 10
C
      CALL QATR(XLOW,XU,0.001,40,FCT,Y,IER,AUX)
C
      T(I)=Y+TIME
      P(I)=XLOW**(3.0*GAMMA)*PP
      XLOW=XLOW-0.020
      IF (XLOW.LT.XAPP) GO TO 3
    2 CONTINUE
    3 TIME=T(I)
      N=I
      WRITE (6,20) I,XAPP,T(I),P(I),PP
```

```
      XL=2.20
C
C     THE SECOND ROOT OF THE CAVITY EQUATION OF MOTION IS
C     FOUND USING SUBROUTINE ZFALSE.
C
      XR=2.40
      ALPHA=PRATIO/(GAMMA-1.0)
C
      CALL ZFALSE (F,0.001,3,XL,XR,XAPP,ITMAX,IER)
C
      PP=PRATIC
      PROOT=XAPP**(3.0*GAMMA)
      PRATIO=PROOT*PRATIC
C
C     INTEGRATION PARAMETERS FOR SUBROUTINE QATR ARE
C     ASSIGNED.
C
      XLOW=1.001
      XL=1.001
      DO 6 I=1,500
      IF (I.EQ.311) GO TO 10
C
      CALL QATR(XLOW,XU,0.001,40,FCT,Y,IER,AUX)
C
      T(I)=Y+TIME
      P(I)=XU**(3.0*GAMMA)*PP
      XL=XL+0.020
      IF (XU.GT.XAPP) GO TO 7
    6 CONTINUE
    7 TIME=T(I)
      N=I
      WRITE (6,20) I,XAPP,T(I),P(I),PP
      GO TO 1
   10 WRITE (6,13)
      DO 11 M=1,310
      WRITE (6,14) M,T(M),P(M)
   11 CONTINUE
C
C     SOLUTION ARRAY IS PREPARED FOR PLOTTING USING SUB-
C     ROUTINE DRAW.
C
      REAL*8 TITLE(12)
      READ (5,15) TITLE
      REAL LABLE/'    '/
C
      CALL DRAW (300,T,P,0,0,LABLE,TITLE,0.0,0.0,0,0,0,6,8
                 ,0,LAST)
C
   13 FORMAT ('1',/////,T25,'NON-DIMENSIONAL TIME',T50,'CAVI
              TY PRESSURE/PRESSURE AT INFINITY')
   14 FORMAT (/,T18,I3,T27,F10.4,T58,F10.4)
   15 FORMAT (6A8)
   19 FORMAT ('1',///,T22,'I',T31,'XAPP',T43,'TIME',T55,'P(I
              )',T68,'PP')
   20 FORMAT (/,20X,I3,4(2X,F10.4))
      STOP
      END


      FUNCTION F(X)
      COMMON GAMMA,ALPHA
      F=-(ALPHA*X**(3.0*GAMMA))+((ALPHA+1.0)*X**3.0)-1.0
      RETURN
      END


      FUNCTION FCT(X)
      COMMON GAMMA,ALPHA
      FCT=(X**(-2.0))*(-(ALPHA*X**(3.0*GAMMA))+((ALPHA+1.0)*
          X**3.0)-1.0)**(-0.5)
      RETURN
      END
```

```
      SUBROUTINE ZFALSE (F,EPS,NSIG,XL,XR,XAPP,ITMAX,IER)
C
      IER = 0
      IC = 0
      EPSP = 10.**(-NSIG)
      FXL = F(XL)
      FXR = F(XR)
      IF (FXL*FXR) 15,10,5
C                                     TERMINAL ERROR
    5 IER = 129
      GO TO 40
C                                     FXL OR FXR = 0
   10 XAPP = XR
      IF (FXL .EQ. 0.0) XAPP = XL
      GO TO 40
C                                     COMPUTE APPROXIMATE ROOT
   15 XAPP = XL+FXL*(XR-XL)/(FXL-FXR)
      FXAPP = F(XAPP)
      IF (ABS(FXAPP) .GT. EPS) GO TO 20
      GO TO 40
C                                     DETERMINE WHETHER APPROXI
C                                     LIES BETWEEN XAPP AND XL
C                                     AND XR
   20 IF (FXAPP*FXL .GT. 0.0) GO TO 25
      XR = XAPP
      FXR = FXAPP
      GO TO 30
   25 XL = XAPP
      FXL = FXAPP
C                                     DETERMINE IF (XR-XL .GT.
   30 IF (XR-XL .GT. EPSP*ABS(XR)) GO TO 35
      GO TO 40
C                                     CONTINUE FOR ITMAX ITERAT
   35 IC = IC+1
      IF (IC.LE.50) GO TO 15
      IER = 130
   40 ITMAX = IC
      IF (IER .NE. 0) GO TO 9000
      GO TO 9005
 9000 CONTINUE
      CALL UERTST (IER,'ZFALSE')
 9005 RETURN
      END
C


      SUBROUTINE UERTST(IER,NAME)
C
      DIMENSION           ITYP(5,4),IBIT(4)
      INTEGER*2           NAME(3)
      INTEGER             WARN,WARF,TERM,PRINTR
      EQUIVALENCE         (IBIT(1),WARN),(IBIT(2),WARF),(IBIT
      DATA      ITYP      /'WARN','ING ',4*'    ',
     *                    'WARN','ING(','WITH',' FIX',')   ',
     *                    'TERM','INAL',4*'    ',
     *                    'NON-','DEFI','NED ',3*'    ',
     *          IBIT      / 32,64,128,0/
      DATA      PRINTR    / 6/
      IER2=IER
      IF (IER2 .GE. WARN) GO TO 5
C                                     NON-DEFINED
      IER1=4
      GO TO 20
    5 IF (IER2 .LT. TERM) GO TO 10
C                                     TERMINAL
      IER1=3
      GO TO 20
   10 IF (IER2 .LT. WARF) GO TO 15
C                                     WARNING(WITH FIX)
      IER1=2
```

```
      GO TO 20
C                                       WARNING
   15 IER1=1
C                                       EXTRACT 'N'
   20 IER2=IER2-IBIT(IER1)
C                                       PRINT ERROR MESSAGE
      WRITE (PRINTR,25) (ITYP(I,IER1),I=1,5),NAME,IER2
   25 FORMAT(' *** I M S L(UERTST) ***  ',5A4,4X,3A2,4X,I2)
      RETURN
      END
//GO.SYSIN DD *
HOLM,D. HYDRAULIC RAM CAVITY
        PRESSURE OSCILLATION
```

## LIST OF REFERENCES


1. Cole, Robert H., Underwater Explosions. Princeton University Press, 1948.

2. NASA Technical Note, D-3143, Investigation of Characteristics of Pressure Waves Generated in Water-Filled Tanks Impacted by High Velocity Projectiles, by F. S. Stepka, C. R. Morse, and R. P. Dengler, December, 1965.

3. NASA Technical Note, D-1537, Preliminary Investigation of Catastrophic Fracture of Liquid-Filled Tanks Impacted by High Velocity Particles, by F. S. Stepka and C. R. Morse, May 1963.

4. NASA Technical Note, D-3456, Projectile-Impact-Induced Fracture of Liquid-Filled, Filament-Reinforced Plastic or Aluminum Tanks, by F. S. Stepka, June 1966.

5. NASA Technical Note, D-3627, Effect of Projectile Size and Material on Impact Fracture of Walls of Liquid-Filled Tanks, by C.R. Morse and F. S. Stepka, September 1966.

6. Naval Weapons Center Technical Publication, 5227, Fluid Analysis of Hydraulic Ram, by E. A. Lundstrom, July 1971.

7. McDonnell Aircraft Engineering Methods Authorization, F65-76-555, Hydraulic Ram: A Fuel Tank Vulnerability Study, R.N. Yurkovich, September 1969.

8. AFFDL-TR-70-43 Vol. 1, Survivable Fuel Tank Systems Selection Technique R & O Handbook Report,Volume 1, by F.M. Cooper and W. S. Reinsch, North American Rockwell Corporation, Los Angeles, California, 1969.

9. Two-Phase Shock Tests of Long Elastic Bodies Performed in a 26" Diameter Air Gun, by R.I. Butler, from Institute of Environmental Sciences Proceedings, 1961.

10. Boeing Company Report No. D162-10294-1, Hydraulic Ram, by R. G. Blaisdell, 18 September 1970.

11. Sedov, L. I., Similarity and Dimensional Methods in Mechanics. Academic Press, New York, 1959.

12. Sommerfeld, Arnold, Mechanics of Deformable Bodies. Academic Press, New York, 1964, Chapter III.

13. Liepman, H. W. and Roshko, A., Elements of Gasdynamics. John Wiley and Son, Inc., New York, 1957, Chapter III.

INITIAL DISTRIBUTION LIST

| | | No. Copies |
|---|---|---|
| 1. | Defense Documentation Center<br>Cameron Station<br>Alexandria, Virginia 22314 | 2 |
| 2. | Library (Code 0212)<br>Naval Postgraduate School<br>Monterey, California 93940 | 2 |
| 3. | Chairman, Department of Aeronautics (Code 57)<br>Naval Postgraduate School<br>Monterey, California 93940 | 1 |
| 4. | Professor A. E. Fuhs, Code 57Fu<br>Department of Aeronautics<br>Naval Postgraduate School<br>Monterey, California 93940 | 15 |
| 5. | LTJG D. P. Holm<br>132 East Oakview Place<br>San Antonio, Texas 78209 | 2 |
| 6. | Mr. Irv Silver, Code 03<br>Naval Air Systems Command<br>Washington, D. C. 20360 | 1 |
| 7. | Dr. Frank Tanczos, Code 03<br>Naval Air Systems Command<br>Washington, D. C. 20360 | 1 |
| 8. | Colonel James Thompson USAF<br>WSEG/IDA<br>400 Army Navy Drive<br>Arlington, Virginia 22202 | 1 |
| 9. | Captain James McNerney<br>DDR & E<br>Pentagon<br>Department of Defense<br>Washington, D. C. 20301 | 1 |
| 10. | CDR Merlin L. Johnson<br>Naval Air Systems Command<br>Washington, D. C. 20360 | 1 |

| | | |
|---|---|---|
| 11. | CDR D. Hicks<br>Naval Air Systems Command<br>Washington, D. C. 20360 | 1 |
| 12. | Robert G. Clodfelter<br>AFAPL<br>Wright-Patterson AFB, Ohio 45433 | 1 |
| 13. | Colonel Florian A. Holm USAF (Ret.)<br>132 East Oakview Place<br>San Antonio, Texas 78209 | 1 |
| 14. | Mrs. W. R. Elniff<br>820 Sunset Drive<br>Lawrence, Kansas 66044 | 1 |
| 15. | LT Laird Stanton<br>SMC 2746<br>Naval Postgraduate School<br>Monterey, California 93940 | 1 |
| 16. | Robert G. Blaisdell<br>Structures R&D Program Manager<br>Boeing Aerospace Group<br>P. O. Box 3999<br>Seattle, Washington 98124 | 1 |

SECURITY CLASSIFICATION OF THIS PAGE (When Data Entered)

| REPORT DOCUMENTATION PAGE | | READ INSTRUCTIONS BEFORE COMPLETING FORM |
|---|---|---|
| 1. REPORT NUMBER | 2. GOVT ACCESSION NO. | 3. RECIPIENT'S CATALOG NUMBER |
| 4. TITLE (and Subtitle)<br>Hydraulic Ram Shock Wave and Cavitation Effects on Aircraft Fuel Cell Survivability | | 5. TYPE OF REPORT & PERIOD COVERED<br>Master's Thesis; September 1973<br>6. PERFORMING ORG. REPORT NUMBER |
| 7. AUTHOR(s)<br>Dwight Patrick Holm | | 8. CONTRACT OR GRANT NUMBER(s) |
| 9. PERFORMING ORGANIZATION NAME AND ADDRESS<br>Naval Postgraduate School<br>Monterey, California 93940 | | 10. PROGRAM ELEMENT, PROJECT, TASK AREA & WORK UNIT NUMBERS |
| 11. CONTROLLING OFFICE NAME AND ADDRESS<br>Naval Postgraduate School<br>Monterey, California 93940 | | 12. REPORT DATE<br>September 1973<br>13. NUMBER OF PAGES<br>84 |
| 14. MONITORING AGENCY NAME & ADDRESS(if different from Controlling Office)<br>Naval Postgraduate School<br>Monterey, California 93940 | | 15. SECURITY CLASS. (of this report)<br>Unclassified<br>15a. DECLASSIFICATION/DOWNGRADING SCHEDULE |

16. DISTRIBUTION STATEMENT (of this Report)

Approved for public release; distribution unlimited.

17. DISTRIBUTION STATEMENT (of the abstract entered in Block 20, if different from Report)

18. SUPPLEMENTARY NOTES

19. KEY WORDS (Continue on reverse side if necessary and identify by block number)

Hydraulic ram
Aircraft Fuel Cell Survivability

20. ABSTRACT (Continue on reverse side if necessary and identify by block number)

Hydraulic ram is the dynamic loading of fuel tanks when impacted by bullets or other projectiles. During impact and penetration of the fuel cell, intense pressure waves are generated by the projectile.

A ballistic range was built and experimental testing was conducted to study hydraulic ram phenomena. A 0.22 caliber rifle was used to accelerate projectiles at velocities in the range of 0.38 km/sec into a transparent, water filled tank. Shape and intensity of the shock wave pressure pulse induced as a result of

DD FORM 1 JAN 73 1473 EDITION OF 1 NOV 65 IS OBSOLETE
S/N 0102-014-6601 |
(Page 1)



SECURITY CLASSIFICATION OF THIS PAGE (When Data Entered)

20. (continued)

projectile impact were determined using a dual shadowgraph system. Peak pressures were found to be as high as $16.8 \times 10^5$ kg/cm$^2$. The rate of energy transfer to the fluid by the projectile was determined experimentally and compared with analytical predictions. A characteristic time was defined establishing the separation point between the shock and cavity phases of hydraulic ram.